A SEMICLASSICAL TRANSPORT MODEL FOR THIN QUANTUM BARRIERS

by

Kyle A. Novak

A dissertation submitted in partial fulfillment of
the requirements for the degree of

Doctor of Philosophy

(Mathematics)

at the

UNIVERSITY OF WISCONSIN–MADISON

2006

Report Documentation Page

Form Approved
OMB No. 0704-0188

1. REPORT DATE **01 JUN 2006**	2. REPORT TYPE **N/A**	3. DATES COVERED **-**

4. TITLE AND SUBTITLE **A Semiclassical Transport Model For Thin Quantum Barriers**	5a. CONTRACT NUMBER 5b. GRANT NUMBER 5c. PROGRAM ELEMENT NUMBER
6. AUTHOR(S)	5d. PROJECT NUMBER 5e. TASK NUMBER 5f. WORK UNIT NUMBER
7. PERFORMING ORGANIZATION NAME(S) AND ADDRESS(ES) **University Of WisconsinMadison**	8. PERFORMING ORGANIZATION REPORT NUMBER
9. SPONSORING/MONITORING AGENCY NAME(S) AND ADDRESS(ES) **AFIT/CIA**	10. SPONSOR/MONITOR’S ACRONYM(S) 11. SPONSOR/MONITOR’S REPORT NUMBER(S)

12. DISTRIBUTION/AVAILABILITY STATEMENT
Approved for public release, distribution unlimited

13. SUPPLEMENTARY NOTES

14. ABSTRACT

15. SUBJECT TERMS

16. SECURITY CLASSIFICATION OF:			17. LIMITATION OF ABSTRACT	18. NUMBER OF PAGES	19a. NAME OF RESPONSIBLE PERSON
a. REPORT **unclassified**	b. ABSTRACT **unclassified**	c. THIS PAGE **unclassified**	**UU**	**77**	

Standard Form 298 (Rev. 8-98)
Prescribed by ANSI Std Z39-18

Abstract

We present a time-dependent semiclassical transport model for mixed-state scattering with thin quantum barriers. The idea is to use a multiscale approach as a means of connecting regions for which a classical description of the system dynamics is valid across regions for which the classical description fails, such as when the gradient of the potential is undefined. We do this by first solving a stationary Schrödinger equation in the quantum region to obtain the scattering coefficients. These coefficients allow us to build an interface condition to the particle flux that bridges the quantum region, connecting the two classical regions. Away from the barrier, the problem may be solved by traditional numerical methods. Therefore, the overall numerical cost is roughly the same as solving a classical barrier.

We construct numerical methods based on this semiclassical approach and validate the model using various numerical examples. In the one-dimensional case, we use a finite-volume method that extends the Hamiltonian-preserving scheme introduced by Jin and Wen for a classical barrier. In the two-dimensional case, we consider a mesh-free particle method that can be computed efficiently and that may be extended to higher-dimensions. The semiclassical transport model is verified numerically by examining the convergence of the Schrödinger and the von Neumann equations to the semiclassical limit for several examples. Finally, we examine an extension of the model to coherent dynamics necessary for periodic crystalline and mesoscopic scale quantum barriers.

Acknowledgments

I would like to thank my advisor, Professor Shi Jin, for his guidance during the past two years. His broad research interests have provided me with a unique appreciation and intuition of several problems in applied mathematics. I am grateful to the other committee members, Professors Slemrod, Milewski, Rossmanith and Han, who have provided invaluable insight and suggestions during my research. I would also like to acknowledge Professors Degond, Gamba and Waleffe for the interesting conversations during the course of this research. Finally, I would like to thank my wife for her support and patience.

O amazement of things—even the least particle!

—Walt Whitman, “Song at Sunset”

Table of Contents

Page

List of Tables

List of Figures

Chapter 1

Introduction

In this work, we develop a semiclassical model of particle dynamics in the presence of a thin quantum barrier. Thin quantum barriers include quantum dot and quantum wire structures, resonant tunneling diodes, thin films, and interfaces between two dissimilar materials such as p-n junctions. Simulation of electron distributions in the presence of such barriers is important to the understanding of the behavior of plasmas, semiconductors, and modern electronic devices. Advances in nanoscale materials fabrication technology have prompted the need for efficient numerical simulation of quantum structures. However, simulation is difficult when the system reacts over different length and time scales since the smaller scale usually drives the accuracy and consistency of the solution. Even when only interested in the macroscopic behavior, one may be forced to resolve the microscopic dynamics. Correspondence principles allow us to extract macroscopic behavior from microscopic dynamics in terms of a weak limit. When the scales act over several orders of magnitude, the numerical solution to the problem at the smallest scale becomes computationally intractable. In these cases, one often relies on a multiscale approach to provide a numerically efficient solution.

An example is the modeling of electron transport in nanostructures, such as resonant tunneling diodes, superlattices or quantum dots, where quantum phenomena in localized regions of the devices cannot be ignored. While one can use quantum mechanics in the entire region, it is clearly more computationally efficient to take a multiscale approach using classical mechanics in the rest of the device by using a domain decomposition technique. Such a model was introduced by Ben Abdallah, Gamba and Degond [6, 7, 8]. In this model, interface conditions connecting the classical and the quantum regions were used to couple two classical regions with a quantum region.

This work is an extension of the Hamiltonian-preserving finite-volume method introduced by Jin and Wen [21, 22] for solving the multi-dimensional classical Liouville equation with a discontinuous (but classical) potential. The idea there was to build an interface condition, such as used in [7], that properly incorporates transmission and reflection information at the barrier into the numerical flux. This produces a scheme that connects momenta (velocities) on both sides of the barrier via the Hamiltonian preservation principle. Such a method is stable in both l^1- and l^∞-norms under a hyperbolic stability condition and captures sharply the weak semiclassical limit of the linear Schrödinger equation or geometrical optics through the barrier or interface.

The quantum barrier that separates the two classical regions differs from a classical barrier in that a quantum wave can tunnel through a barrier, be partially transmitted and reflected by a barrier, and resonate inside a barrier. The method proposed in this thesis is to solve the Schrödinger equation (either exactly or numerically) inside the quantum barrier in order to generate transmission and reflection coefficients, and then use that information in the interface condition to solve the classical Liouville equation through the barrier, in the spirit of the Hamiltonian-preserving method of Jin and Wen. When the quantum barrier is thin (on the order of a de Broglie wavelength), solving the time-independent Schrödinger equation suffices. Thus, the first step is merely preprocessing. Once the transmission and reflection coefficients are generated, the time marching is based on classical mechanics. Hence, this approach, which efficiently handles a thin quantum barrier, has a computational cost similar to a classical simulation in the entire device.

The primary focus of this dissertation is the development and numerical implementation of the semiclassical model. While a model may be rigorously defined mathematically, we are often unable understand its intricacies without computer experiments and simulation. Mathematician Peter Lax once stated "It is impossible to exaggerate the extent to which modern applied mathematics has been shaped and fueled by the general availability of fast computers with large memories. Their impact on mathematics, both applied and pure, is comparable to the role of the telescopes in astronomy and microscopes in biology." [27] Therefore, a secondary focus of this thesis is the simulation of the semiclassical Liouville equation and the von Neumann equation for several examples. In this manner, we are able to both validate and verify the model and also illustrate particle dynamics in a variety of environments.

In Chapter 2 we introduce the semiclassical model. The chapter provides a brief review of the underlying physics and derives the semiclassical limit of the Schrödinger equation. The correspondence between classical and quantum mechanics is discussed. The formal model is developed in terms of the weak Hamiltonian property and an interface condition. Finally, we examine limitations of the model in terms of entropy and time-irreversibility.

In Chapter 3 we propose the implementation of the semiclassical model and its numerical discretization in one-dimension. The one-dimensional interface condition is derived using the transfer matrix method and the model is employed using a finite-volume method. We present four numerical examples to verify the numerical method and validate the semiclassical model. Our numerical results indicate that the model correctly captures the solution of the Schrödinger equation in the entire domain in the limit of the vanishing scaled Planck constant.

In Chapter 4 we extend of the numerical implementation of the semiclassical model to two dimensions. The two-dimensional interface condition is derived using the quantum transmitting boundary method and the model is employed using a mesh-free particle method. We present two numerical examples to verify and validate the semiclassical model and the numerical method. The results indicate that the model correctly captures the Schrödinger solution in the limit semiclassical limit.

In Chapter 5 we discuss corrections to the model for thin barriers to extend it to mesoscopic and periodic barriers. This chapter attempts to circumvent the shortcomings of the model and provide a direction for future research.

Chapter 2

Semiclassical Model

2.1 Correspondence between classical and quantum mechanics

2.1.1 From classical to quantum mechanics

A typical problem under consideration is particle flow in a plasma or through a solid-state device over a macroscopic scale. If the potential is sufficiently smooth we may describe non-interacting particle dynamics in phase space classically as the Hamiltonian system

$$\frac{dx}{dt} = \frac{p}{m} = \nabla_p H(x,p), \quad \frac{dp}{dt} = -\nabla_x V = -\nabla_x H(x,p) \tag{2.1}$$

where $x(t) \in \mathbb{R}^d$ is the particle position, $p(t) \in \mathbb{R}^d$ is the momentum, m is the effective mass and $V(x)$ is a time-independent potential. The Hamiltonian function $H(x,p)$ represents the total energy of the system

$$H(x,p) = \frac{|p|^2}{2m} + V(x) = E. \tag{2.2}$$

One may introduce a probability distribution of particles $f(x,p,t)$ in phase space. By requiring that the probability be conserved along the particle trajectories (the Liouville condition), one has

$$\frac{d}{dt}f = \frac{\partial}{\partial t}f + \frac{dx}{dt}\cdot\nabla_x f + \frac{dp}{dt}\cdot\nabla_p f = 0.$$

With the help of equation (2.1), one gets the classical Liouville equation

$$\frac{\partial}{\partial t}f = \{H,f\} = \nabla_p f\cdot\nabla_x H - \nabla_x f\cdot\nabla_p H \tag{2.3}$$

where $\{\,\cdot\,,\,\cdot\,\}$ is the Poisson bracket. Alternatively,

$$\frac{\partial}{\partial t}f + \frac{p}{m}\cdot\nabla_x f - \nabla_x V(x)\cdot\nabla_p f = 0. \tag{2.4}$$

By considering the zeroth-order moment of $f(x,p,t)$, one obtains the probability position density in physical space

$$\rho(x,t) = \int_{\mathbb{R}^d} f(x,p,t)\,dp,$$

which serves as a primary observable for the comparison of the model.

When the potential fluctuates rapidly over a short distance or the particles impinge on a sharp jump in potential, the classical description fails to capture the quantum wave-like nature of the particle and the Liouville description produces an incorrect solution. In particular, the classical Liouville equation does not model barrier tunneling, probabilistic partial reflection and transmission, or resonance which are crucial to the behavior of many modern electronic devices.

By considering Dirac quantization, one has the formal correspondence between the classical quantities and the quantum operators

$$x \quad\rightarrow\quad x, \qquad\qquad p \quad\rightarrow\quad -i\hbar\nabla, \qquad\qquad \text{and} \qquad\qquad E \quad\rightarrow\quad i\hbar\tfrac{\partial}{\partial t}, \tag{2.5}$$

where $\hbar$ is Planck's constant. Using this quantization, one obtains the Schrödinger equation from the classical Hamiltonian (2.2)

$$i\hbar\frac{\partial}{\partial t}\psi = \hat{H}\psi = \left(-\frac{\hbar^2}{2m}\Delta + V(x)\right)\psi \tag{2.6}$$

which describes the time evolution of the probability amplitude $\psi(x,t;\tilde{x},\tilde{p})$ initially centered at $\tilde{x}$ with an initial energy state $E = H(\tilde{x},\tilde{p})$. The square of the magnitude of the probability amplitude $\rho(x,t) = |\psi(x,t)|^2$ gives the position density in physical space.

Instead of considering a pure state system, one may also consider a mixed state system for which the initial state $H(x,p)$ of the particle is given in terms of a macroscopic statistical distribution $\tilde{f}(x,p)$. Define the density matrix as

$$\hat{\rho}(x,x',t) = \int_{\mathbb{R}^d}\int_{\mathbb{R}^d} \tilde{f}(\tilde{x},\tilde{p})\psi(x,t;\tilde{x},\tilde{p})\overline{\psi}(x',t;\tilde{x},\tilde{p})\,d\tilde{x}\,d\tilde{p}\,. \tag{2.7}$$

The time evolution of the density matrix is found by taking the partial derivative of equation (2.7) with respect to t. By using the Schrödinger equation (2.6) and the hermicity of Hamiltonian operator $\hat{H}$, one obtains the von Neumann equation

$$i\hbar\frac{\partial}{\partial t}\hat{\rho}(x,x',t) = \left(-\frac{\hbar^2}{2m}[\Delta_x - \Delta_{x'}] + V(x) - V(x')\right)\hat{\rho}(x,x',t). \tag{2.8}$$

The formal correspondence between the Liouville equation and the von Neumann equation is seen by replacing the Poisson bracket in equation (2.3) with the commutator

$$\{H,f\} \quad\rightarrow\quad -i\hbar^{-1}[\hat{H},\hat{\rho}]$$

giving

$$i\hbar\frac{\partial}{\partial t}\hat{\rho} = [\hat{H}, \hat{\rho}] = \hat{H}\hat{\rho} - \hat{\rho}\hat{H}. \tag{2.9}$$

which is equivalent to equation (2.8).

The von Neumann representation may be thought of as the fundamental description of quantum mechanics [9]. By taking $\tilde{f}(\tilde{x}, \tilde{p}) = \delta(\tilde{x} - x_0)\delta(\tilde{p} - p_0)$ in (2.7), the density matrix reduces to $\hat{\rho}(x, x', t) = \psi(x, t; x_0, p_0)\overline{\psi}(x', t; x_0, p_0)$ and the physical observables of the mixed state von Neumann equation correspond to those of the pure state Schrödinger equation. In this manner, the Schrödinger equation is simply a limiting case of the von Neumann equation. By taking the diagonal of the density matrix, one gets the position density in physical space

$$\hat{\rho}(x, x, t) = \int_{\mathbb{R}^d}\int_{\mathbb{R}^d} \tilde{f}(\tilde{x}, \tilde{p})|\psi(x, t; \tilde{x}, \tilde{p})|^2 \, d\tilde{x}\, d\tilde{p}.$$

2.1.2 Semiclassical limit: quantum to classical

Consider a characteristic length and time scale $L\delta x$ and $L\delta t$ where δx is the natural length scale such as a de Broglie wavelength $\delta x = \hbar/p$ for some momentum p. By rescaling x, x' and t

$$x \mapsto x/L\delta x, \quad x' \mapsto x'/L\delta x, \quad t \mapsto t/L\delta t$$

in the von Neumann equation we have

$$i\varepsilon\frac{\partial}{\partial t}\hat{\rho}(x, x', t) = \left(-\frac{\varepsilon^2}{2m}[\Delta_x - \Delta_{x'}] + V(x) - V(x')\right)\hat{\rho}(x, x') \tag{2.10}$$

where the dimensionless scaled Planck constant $\varepsilon = [mL(\delta x)^2/\delta t]^{-1}\hbar$ and the effective mass m has been nondimensionalized. Solving the Schrödinger and von Neumann equations numerically presents several difficulties. The de Broglie wavelength must be resolved numerically to ensure correct physical observables of the solution. Typically, this requires that the mesh size $\Delta x = O(\varepsilon)$ or even $o(\varepsilon)$ with a similar constraint on the time discretization Δt [4, 33]. When ε is small, computation is expensive since we need to use $O(N^{d+1})$ operations to compute the Schrödinger solution and $O(N^{2d+1})$ operations to compute the von Neumann solution where $N = O(\varepsilon^{-1})$ is the number of grid points in each space dimension. Because of such reasons, semiclassical methods are important for the solutions when $\varepsilon \ll 1$.

A typical path to the derivation of semiclassical limit is through the WKB approximation. However, the WKB approximation to the Schrödinger equation fails to capture multiphase information beyond caustics [19, 40]. An alternative method is to use the Wigner transform, the Fourier transform of the density matrix,

$$W(x,p,t) = \frac{1}{(2\pi)^d} \int_{\mathbb{R}^d} \hat{\rho}(x + \tfrac{1}{2}\varepsilon y, x - \tfrac{1}{2}\varepsilon y, t) e^{-ip\cdot y}\, dy. \tag{2.11}$$

By applying the transform to the von Neumann equation one has the Wigner equation [43]

$$\frac{\partial}{\partial t} W + \frac{p}{m} \cdot \nabla_x W - \Theta^\varepsilon W = 0$$

where the nonlocal term

$$\Theta^\varepsilon W(x,p,t) = \frac{1}{(2\pi)^d} \int_{\mathbb{R}^d} \frac{i}{\varepsilon} \left[V(x + \tfrac{1}{2}\varepsilon y) - V(x - \tfrac{1}{2}\varepsilon y) \right] \check{W}(x,y,t) e^{-ip\cdot y}\, dy$$

with

$$\check{W}(x,y,t) = \int_{\mathbb{R}^d} W(x,p,t) e^{ip\cdot y}\, dp$$

being the inverse Fourier transform of $W(x,p,t)$. The expression for $\Theta^\varepsilon W$ may also be expressed using the Wigner-Moyal expansion

$$\Theta^\varepsilon W = \nabla_x V \cdot \nabla_p W + \sum_{n=1}^{\infty} \frac{(-1)^n \left(\frac{\varepsilon}{2}\right)^{2n}}{(2n+1)!} \nabla_x^{2n+1} V \cdot \nabla_p^{2n+1} W.$$

When the potential $V(x)$ is sufficiently smooth, one recovers the classical Liouville equation in the limit as $\varepsilon \to 0$ [12, 31]

$$\frac{\partial f}{\partial t} + \frac{p}{m} \cdot \nabla_x f - \nabla_x V \cdot \nabla_p f = 0. \tag{2.12}$$

However, the classical limit is not valid at the discontinuities of the potential [3, 36, 38], where the potential behaves as a quantum scatterer. In the case of a quantum barrier, we may consider a multiscale domain decomposition approach for a solution [7]. In the next section, we present a semiclassical model of a thin quantum barrier with the mixed-state dynamics.

2.2 Particle behavior at a quantum barrier

To model quantum dynamics, we consider a top-down multiscale approach by considering the quantum effects as local corrections to the global classical particle dynamics. In order to isolate and simplify the problem, we make the following assumptions/limitations:

1. The effective width of a barrier is $O(\varepsilon)$. On the classical scale, this means that we may approximate the barrier as having zero width; on the quantum scale, this means that we may typify it as a single scattering center and we may neglect particle dwell time in the quantum region in the semiclassical limit.

2. The distance between neighboring barriers is $O(1)$ and hence each barrier may be considered independently.

3. The change in the potential $\nabla V(x)$ is $O(1)$ except at quantum barriers.

4. The coherence time is sufficiently short and therefore we may neglect interference away from the barrier.

Naturally, one would like to be able to treat a wider class of problems including periodic crystalline domains and mesoscopic barriers for which ε is nonvanishing. We will examine corrections and extensions to these simplifications in Chapter 5.

We begin with the Hamiltonian system discussed in Section 2.1

$$\frac{d}{dt}x = \nabla_p H(x,p), \quad \frac{d}{dt}p = -\nabla_x H(x,p).$$

Let a *bicharacteristic* of the function $H(x,p)$ be the integral curve $\varphi(t) = (x(t), p(t))$. Note that $\varphi(t)$ may not be defined for all time $t \in \mathbb{R}$. When $H(\varphi(t))$ is differentiable,

$$\frac{d}{dt}H(\varphi(t)) = \frac{d}{dt}x \cdot \nabla_x H + \frac{d}{dt}p \cdot \nabla_p H = 0 \tag{2.13}$$

from which it follows that the Hamiltonian is constant along any bicharacteristic $\varphi(t)$, *i.e.,*

$$H(\varphi(t)) = \text{const.} \tag{2.14}$$

Condition (2.13) may be interpreted as the strong form of the conservation of energy, while condition (2.14) may be interpreted as the weak form. If the potential $V(x)$ is discontinuous or not defined in some region $\mathcal{Q} \in \mathbb{R}^d$, the Liouville equation fails to have a global solution since $\nabla_x V(\mathcal{Q})$ is undefined.

The key idea behind Hamiltonian preserving schemes [21, 22] is to (a) solve the Liouville equation locally; (b) use the weak form of the conservation of energy to connect the local solutions together; and (c) incorporate a physically relevant interface condition to choose the correct solution. Let $\mathcal{L}$ be the locally defined set of bicharacteristics of the function $H(x,p)$. By requiring the Hamiltonian to be constant along trajectories, we create an equivalence class of bicharacteristics $[\varphi] = \{\ \varphi^* \in \mathcal{L} \mid H(\varphi^*) = H(\varphi)\ \}$.

Generating a *global bicharacteristic* is a matter of connecting equivalent bicharacteristics at the barriers. Consider the incident and scattered trajectory limits $(x(t^-), p(t^-))$ and $(x(t^+), p(t^+))$ on a barrier in one-dimensional physical space—the two-dimensional case will be considered in Chapter 4. From equation (2.2) the scattered momenta are

$$p(t^+) = -p(t^-) \tag{2.15a}$$

for reflection and

$$p(t^+) = p(t^-)\sqrt{1 + 2m[V(x(t^-)) - V(x(t^+))]/|p(t^{-1})|^2} \tag{2.15b}$$

for transmission. Unless $|p(t^-)|^2 < 2m[V(x(t^+) - V(x(t^-))]$, for which the transmitted momentum is imaginary, the conservation of energy does not tell us which of these two bicharacteristics a particle should physically follow. In order to resolve the nonuniqueness, we require an additional interface condition which we derive from the Schrödinger solution across the interface. By interpreting a wave function as a statistical ensemble of a large number of particles [35], we have the interface condition

$$f(x(t^+), p(t^+)) = R(p_R(t^-))f(x(t^+), p_R(t^-)) + T(p_T(t^-))f(x(t^-), p_T(t^-)) \tag{2.16}$$

where $T(p)$ denotes the probability of an incident particle being transmitted across some region, $R(p)$ denotes the probability of an incident particle being reflected, and the incident momenta

$$\begin{aligned} &p_R(t^-) = -p(t^+) \quad \text{and} \\ &p_T(t^-) = p(t^+)\sqrt{1 + 2m[V(x(t^+) - V(x(t^-))]/|p(t^+)|^2}. \end{aligned}$$

come from equations (2.15b) and (2.15a). The multiple-dimensional interface condition is an extension of the one-dimensional interface condition (2.16) and will be discussed in Section 4.2.

By considering the time-reversibility of the scattering process, we may formulate an alternative but equally valid interface condition

$$f(x(t^-), p(t^-)) = R(p_R(t^+))f(x(t^-), p_R(t^+)) + T(p_T(t^+))f(x(t^+), p_T(t^+)) \tag{2.17}$$

where the scattered momenta $p_R(t^+)$ ans $p_T(t^+)$ are functions of the incident momenta

$$\begin{aligned} &p_R(t^+) = -p(t^-) \quad \text{and} \\ &p_T(t^+) = p(t^-)\sqrt{1 + 2m[V(x(t^-) - V(x(t^+))]/|p(t^-)|^2} \end{aligned}$$

To differentiate between the two interface conditions, we will refer to (2.16) as a *pull* interface condition and (2.17) as a *push* interface condition. The choice between the two equivalent interface conditions is an issue of implementation. An Eulerian method, such as the finite-volume method developed in Section 3.1.2, combines information by pulling information from the appropriate bicharacteristics upwind of the barrier. A Lagrangian method, such as the particle method developed in Section 4.2.3, pushes the information to the appropriate bicharacteristics located downwind of the barrier. Note that the pull interface condition (2.16) is a many-to-one function and the push interface condition (2.17) interface condition is a one-to-many function. In contrast, the scattering for the classical Liouville equations and von Neumann equations are both one-to-one functions.

We assume that the probability of a particle being absorbed by the barrier is zero and hence $T(p) + R(p) = 1$. By defining

$$T(p(t^-)) = \begin{cases} 1 & \text{if } |p(t^-)|^2 > 2m\left[V(x(t^+)) - V(x(t^-))\right] \text{ and} \\ 0 & \text{otherwise,} \end{cases}$$

i.e., total transmission/reflection, condition (2.16) reduces to the classical Liouville condition for which bicharacteristics are uniquely determined for each (x, p). When $T(p) \in (0, 1)$, *i.e.,* partial transmission/reflection, the bicharacteristics are no longer unique and instead we consider multiple bicharacteristic solutions.

Every interaction with a barrier potentially introduces a reflected and transmitted solution resulting in an additional bicharacteristic. We may enumerate the solutions and define a *bicharacteristic solution* to the Liouville equation as

$$f_k(x, p, t) = \int \tilde{f}(\tilde{x}, \tilde{p})\varphi_k(x, p, t; \tilde{x}, \tilde{p})\, d\tilde{x}\, d\tilde{p}$$

where

$$\varphi_k(x, p, t; \tilde{x}, \tilde{p}) = \delta(x(t) - \tilde{x})\delta(p(t) - \tilde{p})$$

is the kth global bicharacteristic for $H(\tilde{x}, \tilde{p})$. By linearity of the Liouville equation we may consider the general solution as the superposition of the bicharacteristic solutions

$$f(x, p, t) = \sum_k s_k(H(x, p)) f_k(x, p, t). \tag{2.18}$$

where $s_k(H(x, p))$ is product of reflection and transmission probabilities along the kth bicharacteristic.

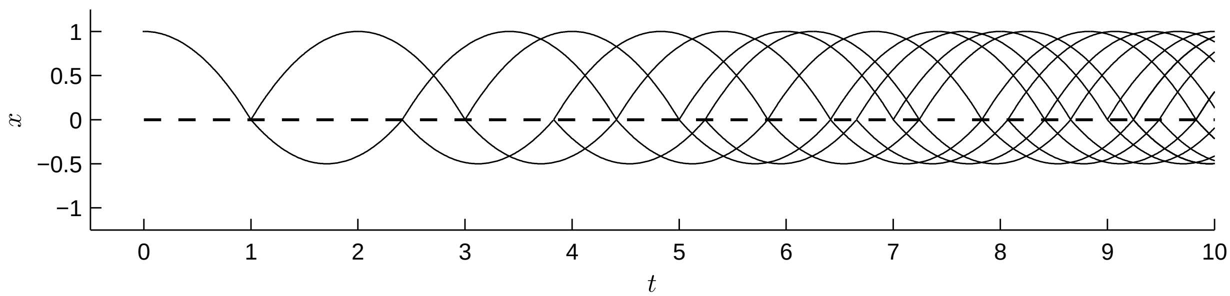

FIGURE 2.1. Particle position as a function of time for potential $V(x) = 2|x| - H(x)$ where $H(x)$ is the Heaviside step function. Particle has initial conditions $\delta(x-1)\delta(p)$.

Except for simple solutions such as the global-in-time solution for a piecewise-constant potential or the local-in-time solution for a piecewise-quadratic potential, an exact solution cannot be explicitly given. Even for a simple discontinuous oscillator the number of bicharacteristics that need to be tracked becomes cumbersome in a short time interval. See Figure 2.2. By solving the model numerically, we mitigate these difficulties.

2.3 Time irreversibility and entropy

The Liouville solution at time t for an initial distribution given by $f(x,p,0)$ is $f(x,p,t) = e^{t\mathcal{L}}f(x,p,0)$ where the Liouville operator $\mathcal{L} = \nabla_p H \cdot \nabla_x - \nabla_x H \cdot \nabla_p$. By reversing the momentum $(p \mapsto -p)$, we have $f(x,-p,t) = e^{-t\mathcal{L}}f(x,-p,0)$ and equivalently $f(x,-p,0) = e^{t\mathcal{L}}f(x,-p,t)$. Hence, the Liouville equation is time reversible under the negation of the momentum. Similarly, the solution of the Schrödinger equation at time t for an initial value $\psi(x,0)$ is $\psi(x,t) = e^{-it\hat{H}}\psi(x,0)$ where the Hamiltonian operator is $\hat{H} = -\frac{\varepsilon^2}{2m}\Delta + V(x)$. By reversing the phase, *i.e.,* by taking the complex conjugate of the probability amplitude $(\psi \mapsto \overline{\psi})$, we have $\psi(x,0) = e^{-it\hat{H}}\psi(x,t)$. Hence, the Schrödinger equation is time-reversible. Unlike the Schrödinger model or the classical Liouville model, the semiclassical Liouville model does not preserve time reversibility.

Consider a statistical ensemble of particles—$f(x,p,0)$ for the Liouville equation and $\psi(x,0)$ for the Schrödinger equation. Suppose that over a some time interval $[0,t]$ this ensemble collides with a barrier resulting in the scattered solutions, $f(x,p,t)$ and $\psi(x,t)$ respectively, consisting of transmitted and reflected parts. Now consider the transmitted and reflected solutions with the momenta and phases reversed as initial conditions, namely $f(x,-p,t)$ and $\overline{\psi}(x,t)$. The time evolution traces backward along the bicharacteristics, striking the barrier and resulting in scattered solutions. The classical Liouville and von Neumann solutions correspond to the original ensemble $f(x,-p,0)$ for and $\overline{\psi}(x,0)$; the semiclassical solution does not. The classical Liouville equation is time reversible because there is only one bicharacteristic for each initial condition. The Schrödinger equation is time reversible because the solution is coherent, containing additional phase information which results in constructive and destructive interference across the barrier. The semiclassical model is not time reversible because it has neither of these properties—the solution is completely decoherent and the bicharacteristics are not unique.

Entropy is a concept closely connected to time irreversiblity. The statistical entropy S of a system is defined as

$$S(t) = \sum_i p_i \log p_i. \tag{2.19}$$

where p_i is the probability of being on the ith local bicharacteristc at time t. Whereas the classical Liouville and the von Neumann equations are isentropic, the semiclassical model is not. As previously stated, the scattering relation for the classical Liouville equations and von Neumann equations are both one-to-one functions, but the scattering relation for the semiclassical model is not. The semiclassical interface condition mixes information from different bicharacteristics, thereby increasing the entropy of the system. The interface condition may be equally posed in terms of a semiclassical scattering matrix

$$\begin{pmatrix} T & R \\ R & T \end{pmatrix}$$

which relates incident and scattered states. The inverse semiclassical scattering matrix

$$\begin{pmatrix} \frac{T}{T-R} & \frac{R}{R-T} \\ \frac{R}{R-T} & \frac{T}{T-R} \end{pmatrix}$$

which solves the time-reversed semiclassical scattering problem will be important in the construction of ghost densities for the slope limiters in the finite-volume method in Section 3.1.2.

As an example, consider the harmonic oscillator with a delta-function barrier

$$V(x) = \tfrac{1}{2}x^2 + \varepsilon\alpha\delta(x)$$

where ε is the scaled Planck constant and α is some parameter. The delta-function quantum barrier transmits a particle with momentum p with probability $[1 + (\alpha/p)^2]^{-1}$ [42]. Furthermore, for the Schrödinger equation, the phase of a transmitted wavepacket are shifted by $\theta_T = -\tan^{-1}(\alpha/p)$ and the phase of a reflected wavepacket is shifted by $\theta_R = \frac{1}{2}\pi + \theta_T$. The phase is also shifted by π when the wavepacket changes direction near ± 1. Take the initial conditions, $f(x, p, 0) = \delta(x-1)\delta(p)$. Then the particle strikes the barrier with momentum $p = 1$ at every time $t = (n + \frac{1}{2})\pi$ for integer n. Let $\alpha = \sqrt{3}$. Then the phase shift is $-\pi/3$ for transmission and $\pi/6$ for reflection. A semiclassical particle with momentum $p = 1$ will be transmitted with probability $\frac{1}{4}$ and reflected with probability $\frac{3}{4}$. Consider the probability of finding the particle in $\mathbb{R}^+$ at $t = 0, \pi, 2\pi, \ldots$. For the semiclassical model, it is

$$1, \quad \tfrac{3}{4}, \quad \tfrac{5}{8}, \quad \tfrac{9}{16}, \quad \tfrac{17}{32}, \quad \tfrac{33}{64}, \quad \tfrac{65}{128}, \quad \ldots$$

because we take each scattering event independently. For the Schrödinger equation, it is

$$1, \quad \tfrac{3}{4}, \quad \tfrac{1}{4}, \quad 0, \quad \tfrac{1}{4}, \quad \tfrac{3}{4}, \quad 1, \quad \ldots$$

because the probability amplitude constructively and destructively interferes with itself. The entropy of the semiclassical system may be calculated using equation (2.19). We have that at $t = n\pi$, the entropy is

$$0, \quad 0.562, \quad 0.661, \quad 0.685, \quad 0.691, \quad 0.6926, \quad 0.6930, \quad \ldots$$

which is a monotonically increasing function asymptotic to the equilibrium value $\log 2$. By time $t = 2\pi$ the semiclassical Liouville solution disagrees with the Schrödinger solution. This discrepancy is due to limitations of the semiclassical model. Clearly, this example violates assumptions 2 and 4 on page 8 that require each interaction with the quantum barrier to be independent.

While the semiclasssical solution is nonisentropic, this does not invalidate the model. Since particles at the classical scale interact with environment, a decoherent, time-irreversible solution is a physically realistic solution. However, a coherent solution is necessary inside a quantum region for mesoscopic and periodic potentials. We shall examine such a model in Chapter 5.

Chapter 3

Semiclassical Model and Numerical Method in One Dimension

3.1 A semiclassical approach

When the quantum barrier is sufficiently narrow, the barrier may be modeled using the time-independent Schrödinger equation. We may then derive the transmission/reflection probabilities for the interface condition (2.16) by considering the current density. The interface condition is used to connect two classical domains modeled by the classical Liouville equation (2.12).

We consider an algorithm consisting of an initialization routine and a Liouville solver:

1. During initialization, we determine the stationary states at the barrier by solving the time-independent Schrödinger equation. The solutions may be found by considering the barrier as an open quantum system [2] outside of which the potential is constant. Typically, this may be done by using a quantum transmitting boundary method [28], a spectral projection method [32], or a transfer matrix method [1, 23, 15]. With this solution, we compute the scattering information, namely the transmission and reflection coefficients.

2. Following initialization, we solve the Liouville equation using a finite volume method. As done in [20] the interface condition (2.16) is built into the numerical flux in a framework called the Hamilton preserving scheme. This yields a numerical scheme for which the stability condition—the CFL condition—is hyperbolic, namely $\Delta t = O(\Delta x, \Delta p)$ with l^∞ and l^1 stability. See [20].

This approach aims at capturing the weak limit of the Schrödinger and von Neumann equations as $\varepsilon \to 0$, without solving the Schrödinger or von Neumann equations over the entire domain, but rather just at the quantum barrier and only in the initialization step. We now discuss the initialization routine and the finite volume routine in detail.

3.1.1 Routine initialization

We use the transfer matrix method because it is robust over a wide range of momenta. On the quantum scale we decompose a one-dimensional barrier into a sequence of step potentials over which we solve the time-independent Schrödinger equation exactly. Take a quantum barrier in the bounded region $\mathcal{Q} = [x_1, x_2]$ and take the potential to be constant outside this barrier—$V(x) = V_1$ in $\mathcal{C}_1 = (-\infty, x_1)$ and $V(x) = V_2$ in $\mathcal{C}_1 = (x_2, \infty)$.

For a state $E = p^2/2m$ the time-independent Schrödinger equation

$$-\varepsilon^2\psi''(x) + 2mV(x)\psi(x) = p^2\psi(x)$$

has the solution

$$\psi(x) = \begin{cases} a_1 e^{i\kappa_1(x-x_1)/\varepsilon} + b_1 e^{-i\kappa_1(x-x_1)/\varepsilon}, & x \in \mathcal{C}_1, \\ \psi_{\mathcal{Q}}, & x \in \mathcal{Q} \\ a_2 e^{i\kappa_2(x-x_2)/\varepsilon} + b_2 e^{-i\kappa_2(x-x_2)/\varepsilon}, & x \in \mathcal{C}_2 \end{cases} \tag{3.1}$$

where $\kappa_{1,2} = \sqrt{p^2 - 2mV_{1,2}}$ and the coefficients a_1, a_2, b_1 and b_2 are uniquely determined by the boundary conditions at x_1 and x_2. By requiring that the solution $\psi(x)$ and its derivative be continuous, $\psi_{\mathcal{Q}}$ is uniquely determined by the values a_1 and b_1 using the boundary conditions $\psi_{\mathcal{Q}}(x_1)$ and $\psi'_{\mathcal{Q}}(x_1)$. In turn, the values a_2 and b_2 are uniquely determined by the values $\psi_{\mathcal{Q}}(x_2)$ and $\psi'_{\mathcal{Q}}(x_2)$. Since the Schrödinger equation is linear, a_2 and b_2 may be expressed as linear functions of a_1 and b_1. Hence, for each momentum p we may relate the solution in $\mathcal{C}_2$ with the solution $\mathcal{C}_1$ in terms of the transfer matrix M

$$\begin{pmatrix} a_2 \\ b_2 \end{pmatrix} = \mathsf{M} \begin{pmatrix} a_1 \\ b_1 \end{pmatrix} = \begin{pmatrix} m_{11} & m_{12} \\ m_{21} & m_{22} \end{pmatrix} \begin{pmatrix} a_1 \\ b_1 \end{pmatrix}. \tag{3.2}$$

An arbitrary quantum barrier may be discretized and approximated by a series of step potentials, for each of which a transfer matrix may be computed analytically. Specifically, the transfer matrix may be approximated as $\mathsf{M} = \mathsf{M}_n \cdots \mathsf{M}_2\mathsf{M}_1$ with $\mathsf{M}_j = \mathsf{D}_{j+1}^{1/2}\mathsf{P}_j\mathsf{D}_j^{1/2}$ where

$$\mathsf{P}_j = \tfrac{1}{2} \begin{pmatrix} 1 + \kappa_j/\kappa_{j+1} & 1 - \kappa_j/\kappa_{j+1} \\ 1 - \kappa_j/\kappa_{j+1} & 1 + \kappa_j/\kappa_{j+1} \end{pmatrix} \tag{3.3}$$

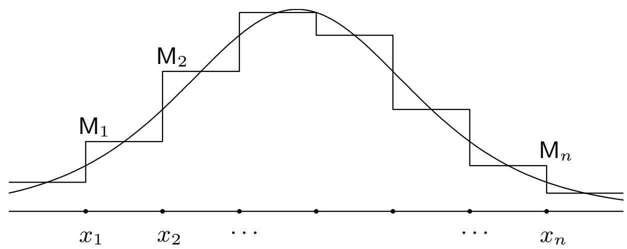

FIGURE 3.1. Approximation of a potential barrier by a series of step potentials. The effective transfer matrix $\mathsf{M} = \mathsf{M}_n \cdots \mathsf{M}_2\mathsf{M}_1$ where M_j is the transfer matrix for a step potential at x_j.

is the transfer matrix associated with a potential jump $V(x_j^+) - V(x_j^-)$ and

$$\mathsf{D}_j = \begin{pmatrix} \exp(i\Delta x\kappa_j/\varepsilon) & 0 \\ 0 & \exp(-i\Delta x\kappa_j/\varepsilon) \end{pmatrix} \tag{3.4}$$

is the transfer matrix associated with the displacement $\Delta x = x_j - x_{j-1}$.

One may also express the solutions in $\mathcal{C}_1$ and $\mathcal{C}_2$ in terms of a scattering matrix S which relates the incident and scattered waves

$$\begin{pmatrix} b_1 \\ a_2 \end{pmatrix} = \mathsf{S}\begin{pmatrix} a_1 \\ b_2 \end{pmatrix} = \begin{pmatrix} r_1 & t_2 \\ t_1 & r_2 \end{pmatrix}\begin{pmatrix} a_1 \\ b_2 \end{pmatrix} = \begin{pmatrix} -m_{21}/m_{22} & 1/m_{22} \\ \Delta/m_{22} & m_{12}/m_{22} \end{pmatrix}\begin{pmatrix} a_1 \\ b_2 \end{pmatrix}. \tag{3.5}$$

where $\Delta = \det \mathsf{M} = m_{22}m_{11} - m_{12}m_{21}$. By considering the time evolution of the position density $\rho(x,t) = |\psi(x,t)|^2$ in the Schrödinger equation, one derives the continuity equation

$$\frac{\partial}{\partial t}\rho \; + \nabla \cdot J = 0$$

where the current-density is defined as $J(x) = \varepsilon m^{-1}\mathrm{Im}\,(\overline{\psi}\nabla\psi)$. From equations (3.1), one has that

$$J(x) = \begin{cases} \kappa_1\left(|a_1|^2 - |b_1|^2\right)/m, & x \in \mathcal{C}_1 \\ \kappa_2\left(|a_2|^2 - |b_2|^2\right)/m, & x \in \mathcal{C}_2 \end{cases} \tag{3.6}$$

where m is the effective particle mass. The positive-valued terms of the $J(x)$ express the flux of right-traveling waves and the negative-valued terms express the flux of left-traveling waves. In particular, for a wave incident on the barrier from the left ($b_2 \equiv 0$), we have $a_2 = t_1a_1$ and $b_1 = r_1a_1$. It follows that the reflection coefficient R_1, the ratio of the reflected to incident current densities, and the transmission coefficient T_1, the ratio of the transmitted to incident current densities, are

$$R_1 = |r_1|^2 \qquad \text{and} \qquad T_1 = (\kappa_2/\kappa_1)|t_1|^2. \tag{3.7}$$

Similarly, for a wave incident from the right

$$R_2 = |r_2|^2 \qquad \text{and} \qquad T_2 = (\kappa_1/\kappa_2)|t_2|^2. \tag{3.8}$$

The transmission and reflection coefficients are uniquely determined along a bicharacteristic. It is clear by time-reversibility that the transmission coefficient along any bicharacteristic is independent of direction

$$T_1(p) = T_2\left(-\sqrt{p^2 + 2m(V_2 - V_1)}\right). \tag{3.9}$$

3.1.2 A second-order finite-volume Liouville solver

Without loss of generality, we shall take the mass $m = 1$ in which case we equate the velocity with the momentum p. To solve the semiclassical Liouville equation (2.12), we use a Hamiltonian-preserving finite-volume method [21]. We consider a uniform mesh in phase space with grid points at $(x_{i+1/2}, p_{j+1/2})$ and denote grid spacing $\Delta x = x_{i+1/2} - x_{i-1/2}$ and $\Delta p = p_{j+1/2} - p_{j-1/2}$ with $i, j \in \mathbb{Z}$. Let the cell centers be $x_i = \frac{1}{2}(x_{i+1/2} + x_{i-1/2})$ and $p_j = \frac{1}{2}(p_{j+1/2} + p_{j-1/2})$. For convenience of notation, we shall take $p_0 \equiv 0$ and $p_{-j} = -p_j$. We shall consider the quantum barrier to be located at a cell interface $x_{Z+1/2}$ for some integer(s) Z.

Define the cell average over the cell $C_{ij} = [x_{i-1/2}, x_{i+1/2}) \times [p_{j-1/2}, p_{j+1/2})$ as

$$f_{ij}^n = \frac{1}{\Delta x \Delta p} \iint_{C_{ij}} f(x, p, t_n)\, dx\, dp.$$

The finite-volume discretization of the one-dimensional Liouville equation (2.12) is

$$f_{ij}^{n+1} = f_{ij}^n - \Delta t \left[p_j \partial_x f_{ij}^n - \partial_x V_i \partial_p f_{ij}^n\right] \tag{3.10}$$

where the discrete operators $\partial_x f_{ij}$, $\partial_p f_{ij}$ and $\partial_x V_i$ are

$$\begin{aligned}
\partial_x f_{ij} &= (f_{i+1/2,j}^- - f_{i-1/2,j}^+)/\Delta x, \\
\partial_p f_{ij} &= (f_{i,j+1/2} - f_{i,j-1/2})/\Delta p, \text{ and} \\
\partial_x V_i &= (V_{i+1/2}^- - V_{i-1/2}^+)/\Delta x
\end{aligned}$$

with

$$f^{\pm}_{i+1/2,j} = \lim_{x\to x^{\pm}_{i+1/2}} \frac{1}{\Delta p}\int_{p_{j-1/2}}^{p_{j+1/2}} f(x,p)\,dp,$$

$$f_{i,j+1/2} = \frac{1}{\Delta x}\int_{x_{i-1/2}}^{x_{i+1/2}} f(x,p_{j+1/2})\,dx, \text{ and}$$

$$V^{\pm}_{i+1/2} = \lim_{x\to x^{\pm}_{i+1/2}} V(x).$$

Upwinding is used to approximate the fluxes $f^{\pm}_{i+1/2,j}$ and $f_{i,j+1/2}$. If the potential $V(x)$ is continuous at some point $x_{i+1/2}$, then $p(t^+) = p(t^-)$ and hence $f^{-}_{i+1/2,j} = f^{+}_{i+1/2,j}$ which reduces the discretized Liouville equation (3.10) to the usual upwind finite volume scheme. At the barrier $x_{Z+1/2}$ special consideration must be taken.

From conservation of the Hamiltonian (2.15) we have that the incident velocity q_j (upwind of the barrier) for a particle transmitted with velocity p_j is

$$q_j = p_j\sqrt{1 + 2(V^{+}_{Z+1/2} - V^{-}_{Z+1/2})/p_j|p_j|}.$$

Similarly, the transmitted velocity (downwind of the barrier) for a particle incident with velocity p_j is $-q_{-j}$. The incident velocity for a particle reflected with velocity p_j is simply $-p_j$. Note that, whereas $-p_{-j} = p_j$, in general $-q_{-j} \neq q_j$. Further note that by time reversibility $T(q_{-j}) = T(p_j)$ and $R(q_{-j}) = R(p_j)$.

The left and right limits of the probability distribution f in the cells immediately downwind of the quantum barrier are determined by the interface condition (2.16)

$$\begin{aligned} f^{+}_{Z+1/2,j} &= R(q_j)f^{+}_{Z+1/2,-j} + T(q_j)f(x^{-}_{Z+1/2},q_j) \qquad \text{for } j>0 \\ f^{-}_{Z+1/2,j} &= R(q_j)f^{-}_{Z+1/2,-j} + T(q_j)f(x^{+}_{Z+1/2},q_j) \qquad \text{for } j<0. \end{aligned}$$

The values for $f(x^{\pm}_{Z+1/2},q_j)$ are approximated in a manner similar to Scheme II of [21]. Consider the flux incident from the left ($q_j > 0$)—the same treatment applies to flux incident from the right. We define $f(x^{-}_{Z+1/2},q_j)$ as the cell average

$$f(x^{-}_{Z+1/2},q_j) = \frac{1}{p_j\Delta p}\int_{q_{j-1/2}}^{q_{j+1/2}} pf(x^{-}_{Z+1/2},p)\,dp \tag{3.11}$$

where

$$q_{j\pm1/2} = \sqrt{p^2_{j\pm1/2} + 2(V^{+}_{Z+1/2} - V^{-}_{Z+1/2})}.$$

The integral is approximated by a composite mid-point rule. Since the limits of the integral are not generally gridpoints in the p-direction, some care must be taken. If $p_{k-1/2} \leq q_{j-1/2} < q_{j+1/2} \leq p_{k+1/2}$ for some k, then we take

$$f(x^-_{Z+1/2}, q_j) = f^-_{Z+1/2,k} + q_j \sigma_p(f^-_{Z+1/2,k})$$

where the slope $\sigma_p(\cdot)$ in the p-direction is calculated using the van Leer limiter

$$\sigma_p(f_{ij}) = \left(\frac{f_{ij} - f_{i,j-1}}{\Delta p}\right) \phi \left(\frac{f_{i,j+1} - f_{ij}}{f_{ij} - f_{i,j-1}}\right) \tag{3.12}$$

with $\phi(\theta) = (\theta + |\theta|)/(1 + |\theta|)$ [29]. Otherwise $p_{k-1/2} \leq q_{j-1/2} < \cdots < q_{j+1/2} \leq p_{k+s+1/2}$ for some k and s, and we take

$$\begin{aligned} f(x^-_{Z+1/2}, q_j) &= \\ &\frac{1}{p_j \Delta p} \Big\{ (p_{k+1/2} - q_{j-1/2}) \Big[p_k f^-_{Z+1/2,k} + \tfrac{1}{2}(p_{k+1/2} + q_{j-1/2}) \sigma_p(p_k f^-_{Z+1/2,k}) \Big] \\ &\qquad + p_{k+1} \Delta p f^-_{Z+1/2,k+1} + \cdots + p_{k+s-1} \Delta p f^-_{Z+1/2,k+s-1} \\ &+ (q_{j+1/2} - p_{k+s-1/2}) \Big[p_{k+s} f^-_{Z+1/2,k+s} + \tfrac{1}{2}(p_{k+s-1/2} + q_{j+1/2}) \sigma_p(p_{k+s} f^-_{Z+1/2,k+s}) \Big] \Big\}. \end{aligned} \tag{3.13}$$

For a second-order accurate method we use a slope-limited piecewise-linear interpolant to approximate the right and left density limits

$$f^{\pm}_{i\mp 1/2,j} = f_{ij} \mp \tfrac{1}{2}(1 - \lambda_j) \Delta x \sigma_x(f_{ij}) \tag{3.14}$$

where $\lambda_j = |v_j| \Delta t / \Delta x$ and the slope $\sigma_x(\cdot)$ in the x-direction is calculated using the van Leer limiter

$$\sigma_x(f_{ij}) = \left(\frac{f_{ij} - f_{i-1,j}}{\Delta x}\right) \phi \left(\frac{f_{i+1,j} - f_{ij}}{f_{ij} - f_{i-1,j}}\right). \tag{3.15}$$

Since the slope $\sigma_x(\cdot)$ is a function of $f_{i-1,j}$, $f_{i,j}$ and $f_{i+1,j}$ and the density f is not necessarily continuous across the barrier in the x-direction, we can not directly use (3.14) and (3.15) to calculate the density limits at the barrier interface. Rather, we first need to construct the ghost densities f^*_Z and f^*_{Z+1} across the barrier using the scattered densities at x_Z and x_{Z+1} based on conservation of mass. Specifically, downwind of the barrier

$$f^+_{Z+1/2} \equiv f^+_{Z+1/2}(f^*_Z, f_{Z+1}, f_{Z+2}) \quad \text{and} \quad f^-_{Z+1/2} \equiv f^-_{Z+1/2}(f_{Z-1}, f_Z, f^*_{Z+1})$$

with ghost densities f^*_Z and f^*_{Z+1} located upwind of the barrier; and upwind of the barrier

$$f^+_{Z-1/2} \equiv f^+_{Z-1/2}(f_{Z-1}, f_Z, f^*_{Z+1}) \quad \text{and} \quad f^-_{Z+3/2} \equiv f^-_{Z+3/2}(f^*_Z, f_{Z+1}, f_{Z+2})$$

with ghost densities f_Z^* and f_{Z+1}^* located downwind of the barrier.

Construction of the ghost densities is analogous to using ghost cells to enforce inflow and outflow semipermeable reflecting boundary conditions. To calculate the ghost densities *upwind* of the barrier we use the interface condition (2.16) to mix together the densities upwind of the barrier that will subsequently be combined through transmission and reflection. In this case

$$\begin{aligned} f_{Z,j}^* &= R(q_j) f_{Z+1,-j} + T(q_j) f(x_Z, q_j) && \text{for } j > 0, \\ f_{Z+1,j}^* &= R(q_j) f_{Z,-j} + T(q_j) f(x_{Z+1}, q_j) && \text{for } j < 0. \end{aligned}$$

To calculate the ghost densities *downwind* of the barrier we unmix the densities downwind of the barrier that were previously combined through transmission and reflection at the barrier. In this case

$$\begin{aligned} f_{Z+1,j}^* &= \frac{T(p_j) f(x_{Z+1}, -q_{-j}) - R(p_j) f_{Z,-j}}{T(p_j) - R(p_j)} && \text{for } j > 0, \\ f_{Z,j}^* &= \frac{T(p_j) f(x_Z, -q_{-j}) - R(p_j) f_{Z+1,-j}}{T(p_j) - R(p_j)} && \text{for } j < 0. \end{aligned}$$

The densities $f(x_{Z+1}, \pm q_{\pm j})$ and $f(x_Z, \pm q_{\pm j})$ are approximated in a manner similar to definition (3.11).

To approximate $f_{i,j+1/2}^{\pm}$ to second-order in the p-direction we have

$$f_{i,j\mp 1/2}^{\pm} = f_{i,j} \mp \tfrac{1}{2}(1 - \lambda_i)\Delta p \sigma_p(f_{ij})$$

with $\lambda_i = |\partial_x V_i| \Delta t / \Delta p$ and the slope $\sigma_p(\cdot)$ defined using the van Leer limiter (3.12).

3.2 Numerical examples

In this section we present a few examples of both pure state dynamics and mixed state dynamics in order to verify and validate the semiclassical model and numerical scheme.

For a mixed state solution with a macroscopic distribution, we are not limited by the support of the wavepacket, and the complexity of the scheme is $O((\Delta x \Delta p \Delta t)^{-1})$ where Δx, Δp, and $\Delta t \gg \varepsilon$. For direct simulation of the von Neumann equation, not only must we resolve ε in space and time but we must solve the equation over two space dimensions and one time dimension so the complexity of the scheme is $O(\varepsilon^{-3})$. When $\varepsilon \ll 1$, the computing time for a direct von Neumann solution is considerably longer than for the multiscale semiclassical Liouville solution.

The numerical Schrödinger solution may be computed using the Crank-Nicolson operator

$$\psi(x_i, t + \Delta t) = (1 + i\varepsilon^{-1}\Delta t H_D)^{-1}(1 - i\varepsilon^{-1}\Delta t H_D)\psi(x_i, t) \tag{3.16}$$

where the discrete Hamiltonian operator

$$H_D = \frac{-\varepsilon^2}{2m}\frac{\delta_{i,i-1} - 2\delta_{ii} + \delta_{i,i+1}}{(\Delta x)^2} + V(x_i) \tag{3.17}$$

with Kronecker delta $\delta_{ii} = 1$ and $\delta_{ij} = 0$ if $i \neq j$. Markowich, Pietra and Pohl [33] show that for such a scheme, in order to guarantee correct approximation to observables for small ε, one needs to take $\Delta x = o(\varepsilon)$ and $\Delta t = o(\varepsilon)$. One may also compute the numerical Schrödinger solution using a pseudospectral method with Strang splitting [4]. In this case, one splits the kinetic and potential terms, so that for each time step

$$\psi(x, t + \Delta t) = e^{\Delta t B/2}\mathcal{F}^{-1}\left[e^{\Delta t A}\mathcal{F}\left[e^{\Delta t B/2}\psi(x,t)\right]\right]$$

where

$$A = \frac{\varepsilon}{2mi}k^2 \qquad \text{and} \qquad B = \frac{1}{i\varepsilon}V(x)$$

and the operators $\mathcal{F}$ and $\mathcal{F}^{-1}$ denote the one-dimensional discrete Fourier transform and discrete inverse Fourier transform with respect to the x and k variables. One can use a mesh that is coarser than the mesh required by a finite-difference method to resolve ε and capture the correct dynamics [4, 5]. Based on numerical observation, we find that we require $\Delta x < \varepsilon/4$ to ensure numerical convergence to the correct physical observables and for numerical error to be insignificant. When the potential is discontinuous, we find that the solution exhibits artificial oscillations unless $\Delta t < (\Delta x)^2/\varepsilon$ and $\Delta t < \varepsilon/V(x)$.

The von Neumann equation

$$i\varepsilon\frac{\partial}{\partial t}\hat{\rho} = \hat{H}\hat{\rho} - (\hat{H}\hat{\rho}^T)^T \qquad \text{with} \qquad \hat{H} = -\frac{\varepsilon^2}{2m}\partial_{xx} + V(x)$$

has the formal solution

$$\hat{\rho}(x, x', t + \Delta t) = e^{i\varepsilon\Delta t\hat{H}}\hat{\rho}(x, x', t)e^{-i\varepsilon\Delta t\hat{H}}.$$

By using the discrete Hamiltonian operator (3.17), we may approximate the von Neumann solution in terms of the Crank-Nicolson operator (3.16) to get a method without splitting error

$$\hat{\rho}_{ij}^{n+1} = (1 + i\varepsilon^{-1}\Delta t H_D)^{-1}(1 - i\varepsilon^{-1}\Delta t H_D)\hat{\rho}_{ji}^* \quad \text{with}$$
$$\hat{\rho}_{ij}^* = (1 - i\varepsilon^{-1}\Delta t H_D)^{-1}(1 + i\varepsilon^{-1}\Delta t H_D)\hat{\rho}_{ji}^n$$

where $\rho_{ij}^n = \hat{\rho}(x_i, x_j', t_n)$. We may also solve the von Neumann equation using a pseudospectral method with Strang splitting [17],

$$\hat{\rho}^{n+1} = e^{\Delta t B/2} \mathcal{F}^{-1} \left(e^{\Delta t A} \mathcal{F} \left(e^{\Delta t B/2} \hat{\rho}^n \right) \right)$$

where

$$A = \frac{\varepsilon}{2mi}(k^2 - k'^2) \qquad \text{and} \qquad B = \frac{1}{i\varepsilon}(V(x) - V(x'))$$

and the operators $\mathcal{F}$ and $\mathcal{F}^{-1}$ denote the two-dimensional discrete Fourier transform and discrete inverse Fourier transform with respect to the (x, x') and (k, k') variables. The FFTs may be optimized by exploiting the hermicity of the density matrix.

Alternatively, we may calculate the von Neumann solution indirectly by solving the Schrödinger equation for several states and then using definition (2.7) to construct the density matrix. This simplifies a two-dimensional problem over N^2 gridpoints to n independent one-dimensional problems over N gridpoints. If the initial distribution is localized in phase space, n may be chosen to be appreciably smaller than N, saving not only memory but also contributing to a considerable reduction in computation time. Furthermore, this approach allows us to implement the solution using a parallel computer cluster. One way to implement such a scheme is to use states generated by taking thin slices of the initial distribution along the x-direction. Consider the WKB initial condition

$$\psi(x, 0; \tilde{x}, \tilde{p}) = (\sigma_x \sqrt{2\pi})^{-1/4} \exp(-(x - \tilde{x})^2 / 4\sigma_x^2) \exp(i\tilde{p}x/\varepsilon), \tag{3.18}$$

which describes a wave packet with an $O(1)$ spread in position and $O(\varepsilon)$ spread in momentum. Let the weight distribution in the definition of the density matrix (2.7) be

$$\tilde{f}(\tilde{x}, \tilde{p}) = \delta(\tilde{x} - x_0) \exp(-(\tilde{p} - p_0)^2 / 2s_\varepsilon^2 \sigma_p^2) / (s_\varepsilon^2 \sigma_p \sqrt{2\pi}) \tag{3.19}$$

where the scaling factor $s_\varepsilon = 1/\sqrt{1 + (\varepsilon/2\sigma_x\sigma_p)^2}$. Then

$$\begin{aligned}
\hat{\rho}(x, x', 0) &= \iint_{-\infty}^{\infty} \tilde{f}(\tilde{x}, \tilde{p}) \psi(x, 0; \tilde{x}, \tilde{p}) \overline{\psi}(x', 0; \tilde{x}, \tilde{p}) \, d\tilde{x} \, d\tilde{p} \\
&= \frac{1}{\sigma_x \sqrt{2\pi}} \exp\left(-\frac{(x - x_0)^2 + (x' - x_0)^2}{4\sigma_x^2} - \frac{(x - x')^2}{2\varepsilon^2 s_\varepsilon^{-2} \sigma_p^{-2}} - \frac{ip_0(x - x')}{\varepsilon} \right) \\
&= \frac{1}{\sigma_x \sqrt{2\pi}} \exp\left(-\frac{(\frac{1}{2}(x + x') - x_0)^2}{2\sigma_x^2} - \frac{(x - x')^2}{2\varepsilon^2 \sigma_p^{-2}} - \frac{ip_0(x - x')}{\varepsilon} \right).
\end{aligned}$$

Using the Wigner transform (2.11), we have the equivalent Liouville initial distribution

$$f(x,p,0) = \frac{1}{2\pi\sigma_x\sigma_p} \exp\left(-\frac{(x-x_0)^2}{2\sigma_x^2} - \frac{(p-p_0)^2}{2\sigma_p^2}\right) \tag{3.20}$$

which is independent of ε.

To compare the convergence of the Schrödinger and von Neumann solution in the semiclassical limit, we use the L^1-error of the position probability density function (pdf),

$$\int_{-\infty}^{\infty} \left|\rho(x,t) - |\psi(x,t)|^2\right| \, dx$$

with $\rho(x,t) = \int_{-\infty}^{\infty} f(x,p,t)\, dp$. We replace $|\psi(x,t)|^2$ with $\hat{\rho}(x,x,t)$ for the von Neumann solution. The semiclassical Liouville model should also predict the correct weak limit for multiphase solutions when interference in the Schrödinger and von Neumann solutions produce oscillations in the probability density distribution. To measure the weak convergence in the semiclassical limit, we determine the L^1-error in the cumulative distribution function (cdf), *i.e.,* the antiderivative of position density [14]

$$\int_{-\infty}^{\infty} \left| \int_{-\infty}^{x} \rho(s,t) - |\psi(s,t)|^2 \, ds \right| \, dx.$$

In each example we compare the exact or numerical semiclassical Liouville solution with numerical Schrödinger or von Neumann solutions for equivalent initial distributions and potentials. Since the interactions with the boundaries are not relevant to the study, a sufficiently large domain is chosen and simulation is stopped before the wave envelope reaches the boundaries.

3.2.1 Schrödinger $O(1)$ wave envelope with a step potential

Consider the step potential

$$V(x) = \begin{cases} 0 & \text{if } x < 0, \\ \frac{1}{2} & \text{if } x > 0. \end{cases} \tag{3.21}$$

A particle impinging on this potential from the left is totally reflected when the incident velocity is less than 1.

We find the exact solution by the method of characteristics by tracing along the bicharacteristics backward in time to the initial conditions. Let $\Omega(t) = \{\ (x,p) \mid x < 0 \text{ and } x - pt < 0, \text{ or } x > 0 \text{ and } x - pt > 0\ \}$ be the region in phase space where the bicharacteristics have not crossed the quantum barrier at $x = 0$ within a time t. Then the exact solution

$$f(x,p,t) = \begin{cases} f(x - pt, p, 0), & (x,p) \in \Omega(t) \\ T \cdot f\left(\dfrac{q}{p}x - qt, q, 0\right) + R \cdot f\left(-x + pt, -p, 0\right), & \text{otherwise} \end{cases} \tag{3.22}$$

where the incident velocity is given by $q = \sqrt{p^2+1}$ if $p > 0$ and $q = -\sqrt{p^2-1}$ if $p \leq 0$. From equations (3.3) and (3.7), the reflection coefficient is given by

$$R = \left|\frac{p-q}{p+q}\right|^2 = |p-q|^4.$$

Note that when $p \in [-1, 0]$, q is imaginary and $R = 1$ indicating total reflection.

Consider the WKB initial condition

$$\psi(x,0) = A(x)e^{iS(x)/\varepsilon}$$

as a wavepacket generalization with the amplitude and phase functions given by

$$\begin{aligned} A(x) &= (\pi\sigma^2)^{-1/4}e^{-(x-x_0)^2/2\sigma^2} \\ S(x) &= ax^2 + bx + c. \end{aligned}$$

Since $S(x)$ is a quadratic function, we can calculate the Wigner transform of $\psi(x,0)$ exactly to get

$$f(x,p,0) = (\pi\varepsilon)^{-1}e^{(x-x_0)^2/\sigma^2}e^{-(2ax+b-p)^2/(\varepsilon/\sigma)^2}.$$

In the semiclassical limit ($\varepsilon \to 0$), we have

$$\begin{aligned} f(x,p,0) &= A^2(x)\delta(p - \nabla_x S(x)) \\ &= (\sigma\sqrt{\pi})^{-1}e^{-(x-x_0)^2/\sigma^2}\delta(p - (2ax+b)). \end{aligned} \tag{3.23}$$

By taking $\sigma = O(1)$ in $A(x)$, we create a wave envelope that is independent of ε, allowing us to study the convergence of solutions as $\varepsilon \to 0$. When $a \neq 0$, the distribution of phases included in the Schrödinger solution is also $O(1)$.

Using the above semiclassical WKB initial conditions (3.23), we note that when $t = -1/2a$ the position density for the Liouville solution (3.22) exhibits a caustic with all bicharacteristics intersecting at either $x = b/2a$, or $x = -b/2a$ for reflected solutions. Because of the nonlinear change to the incident velocities, the transmitted bicharacteristics do not cross simultaneously resulting in a traveling front, the leading edge of which is unbounded.

Take $(x_0, p_0) = (-\frac{1}{2}, 1)$ and take $a = -\frac{1}{4}$, $b = p_0 - 2a = \frac{3}{2}$ and $\sigma = \frac{1}{10}$. Then we have the initial conditions

$$\psi(x, 0) = (10/\pi)^{1/4} \, e^{-100(x-x_0)^2} e^{i(ax^2 + (p_0 - 2ax_0)x)\varepsilon}$$

for the Schrödinger equation and

$$f(x, p, 0) = (10/\pi)^{1/2} \, e^{-200(x-x_0)^2} \delta(p - p_0 - 2a(x - x_0))$$

for the semiclassical Liouville equation. The numerical Schrödinger solution is solved using a Crank-Nicolson finite-difference method over the domain $[-1, 1]$ with mesh size $\Delta x = \Delta t = 10^{-6}$. The exact semiclassical Liouville solution is solved by tracking characteristics forward in time with values determined by the initial velocity given by $\nabla S = \frac{3}{4} - \frac{1}{2}x$. We compute the solution at time $t = 0.8$.

The position densities for several values of ε are shown in Figure 3.2. The convergence results of the errors in the two solutions are listed in Table 3.1. Based on this study, we find that the l^1 convergence rate in ε of the pdf is about 0.6 and the l^1 convergence rate in ε of the cdf is about 1.1.

3.1. Errors in solutions of Example 3.2.1 for different values of ε.

ε	200^{-1}	800^{-1}	3200^{-1}	12800^{-1}
l^1-error (pdf)	8.78×10^{-1}	3.37×10^{-1}	1.55×10^{-1}	8.61×10^{-2}
l^1-error (cdf)	5.15×10^{-2}	1.00×10^{-2}	2.28×10^{-3}	1.08×10^{-4}

3.2.2 Von Neumann solution with step potential

We now consider the solution to the von Neumann equation with the step potential given Example 3.2.1. To construct a von Neumann initial condition $\hat{\rho}(x, x', 0)$ which corresponds to a Liouville initial condition $f(x, p, 0)$, we may directly use the definition of the density matrix (2.7) for some weight function with the probability amplitudes $\psi(x, t)$ given by Gaussian ε-wavepackets

$$\psi(x, 0) = (\pi\varepsilon)^{-1/4} e^{-(x-x_0)^2/2\varepsilon} e^{ip_0 x/\varepsilon}. \tag{3.24}$$

The Liouville initial condition may subsequently be calculated by a Wigner transform of the density matrix. Alternatively, we may construct the density matrix by using the inverse Wigner transform applied to the Liouville initial conditions $f(x,p,0)$ to get

$$\hat{\rho}(x,x',0) = \int_{-\infty}^{\infty} f(\tfrac{1}{2}(x+x'),p,0)e^{ip(x-x')/\varepsilon}\,dp.$$

By taking the Liouville initial conditions to be the Gaussian

$$f(x,p,0) = \frac{1}{2\pi\sigma_x\sigma_p}\exp\left(\frac{-(x-x_0)^2}{2\sigma_x^2}\right)\exp\left(\frac{-(p-p_0)^2}{2\sigma_p^2}\right) \tag{3.25}$$

we may compute the von Neumann initial conditions exactly to get

$$\hat{\rho}(x,x',0) = \frac{1}{\sigma_x\sqrt{2\pi}}\exp\left(-\frac{(\frac{1}{2}(x+x')-x_0)^2}{2\sigma_x^2} - \frac{(x-x')^2}{2\varepsilon^2\sigma_p^{-2}} - \frac{ip_0(x-x')}{\varepsilon}\right). \tag{3.26}$$

We chose $\sigma_x = \sigma_p = 0.05$, $x_0 = -0.5$ and $p_0 = 1.0$ and compared the solutions to the von Neumann and semiclassical Liouville equations at time $t = 1.0$. The von Neumann equation was solved using the psuedospectral method with Strang splitting over the domain $[-1,1]$ with $\varepsilon = 64^{-1}$, 128^{-1}, 256^{-1} and 512^{-1}. The grid spacing was fixed at $\Delta x = 2048^{-1}$ with $\Delta t = (\Delta x)^2/\varepsilon$ to ensure consistency and stability. The exact solution to the semiclassical Liouville model is calculated using equation (3.22).

The position densities for the semiclassical Liouville solution and the von Neumann solution for several values of ε are shown in Figure 3.3. The errors in the two solutions are listed in Table 3.2. Based on our study, we find the convergence rate of the l^1-error of the pdf is about 0.7 as $\varepsilon \to 0$ and the convergence of the l^1-error of the cdf is about 0.9 as $\varepsilon \to 0$.

3.2. Errors in solutions of Example 3.2.2 for different values of ε .

ε	64^{-1}	128^{-1}	256^{-1}	512^{-1}
l^1-error (pdf)	6.03×10^{-1}	4.04×10^{-1}	2.50×10^{-1}	1.40×10^{-1}
l^1-error (cdf)	9.22×10^{-2}	4.83×10^{-2}	2.53×10^{-2}	1.32×10^{-2}

We may also consider the effect of incorporating barrier time delay in the approximation of the von Neumann equation for nonvanishing ε. As evident from the offset of the centers of the distributions on the left side of Figure 3.3, one source of error is the time delay which vanishes in the semiclassical limit. The time delay may be considered as an $O(\varepsilon)$ correction and hence we may neglect it in the semiclassical limit. While the the addition of a delay time is numerically nontrivial, for the analytic solution (3.22) it is a straight-forward modification.

Typically, time delay is defined in terms of the Wigner time delay, the delay to the group velocity of a wave packet resulting from reflection and transmission. As such it is meaningful when the wave packet has a well-defined peak. This is not generally the case, especially when the barrier is sufficiently wide. Considering the scattering relation (3.5), the reflection and transmission group delay times for unit mass are [35]

$$\tau_t = \frac{\varepsilon}{p}\frac{d}{dp}\arg t = \frac{\varepsilon}{p}\mathrm{Im}\,(\frac{1}{t}\frac{dt}{dp}) \qquad \text{and} \qquad \tau_r = \frac{\varepsilon}{p}\frac{d}{dp}\arg r = \frac{\varepsilon}{p}\mathrm{Im}\,(\frac{1}{r}\frac{dr}{dp}).$$

For the step potential (3.21), we have from equation (3.3) that the reflection time delay is

$$\tau_r = 2\varepsilon\mathrm{Im}\,[(pq)^{-1}] = \frac{2\varepsilon}{p\sqrt{1-p^2}}$$

when $p \in [-1, 0]$. There is no transmission or reflection delay time for $p \notin [-1, 0]$. To incorporate the time delay, we make the replacement

$$f\,(-x + pt, -p, 0) \quad \rightarrow \quad f\,(-x + p(t + \tau_r), -p, 0)$$

in the reflected term of the exact solution (3.22).

We compare the von Neumann solution with the Liouville solution with time delay correction. The l^1-errors are listed in Table 3.3. Based on this study, we find that the addition of delay time provides some improvement to the model. The convergence rate of the l^1-error of the pdf is about 1.3 and convergence rate of the l^1-error of the cdf is about 0.9 as $\varepsilon \to 0$.

3.3. Errors in solutions of Example 3.2.2 with time delay correction.

ε	64^{-1}	128^{-1}	256^{-1}	512^{-1}
l^1-error (pdf)	3.67×10^{-1}	1.78×10^{-1}	7.05×10^{-2}	2.23×10^{-2}
l^1-error (cdf)	2.62×10^{-2}	1.65×10^{-2}	7.80×10^{-3}	3.90×10^{-3}

3.2.3 Von Neumann solution with two step potentials

We may consider more complicated geometries by considering multiple barriers. In this example we construct an $O(1)$-wide rectangular barrier by taking two step barriers sequentially. Consider

$$V(x) = \begin{cases} \frac{1}{2} & \text{if } x \in [0, \frac{1}{5}], \\ 0 & \text{otherwise.} \end{cases}$$

We take the initial conditions given in equations (3.25) and (3.26) with $\sigma_x = \sigma_p = 0.05$, $x_0 = -0.45$ and $p_0 = 1.1$. We compute over the domain $[-1.25, 1.25]$ and compare the solutions at time $t = 1.2$. The von Neumann equation is solved using a pseudospectral method with Strang splitting as in Example 3.2.2. The semiclassical Liouville solution is solved using the numerical method proposed in Section 3.1 using N grid points in x and p and $1.5N$ steps in time. The results are shown in Figure 3.4 with $\varepsilon = 0.002$. Even with a fairly coarse mesh, the numerical semiclassical solution agrees well with the von Neumann equation both in the strong limit away from the barrier and in the weak limit between the two step potentials. See Figure 3.5.

We calculate convergence rate as Δx, Δp, $\Delta t \to 0$ of numerical scheme for the semiclassical Liouville equation by computing the l^1-error of the numerical solutions using a mesh with $N = 50$, 100, 200, and 400 grid points. For an "exact" solution, we use the numerical solution using $N = 3200$. The errors are listed in Table 3.4. Based on this study, we find the convergence rate of the numerical scheme using the l^1-norm is about 1.2.

3.4. Errors in solutions of Example 3.2.3 for various mesh sizes Δx.

grid points	50	100	200	400
l^1-error	3.32×10^{-1}	1.15×10^{-1}	4.72×10^{-2}	2.56×10^{-2}

3.2.4 Resonant tunneling von Neumann solution

We present a final example to illustrate a specific physical model, the resonant tunneling diode (RTD) [24, 34, 41]. An RTD consists of thin layers (a few nanometers thick) of different semiconductors, such as gallium arsenide (GaAs) and aluminum gallium arsenide (AlGaAs), that are sandwiched together to form a double-barrier quantum well structure. For semiconductors the de Broglie wavelength is on the order of tens of nanometers, so the length of the entire RTD structure is on the length scale of a de Broglie wavelength. The region outside the barrier is doped to provide a sufficient number of free electrons. Unlike the transmission probabilities of the step potentials presented the previous examples, the transmission probability of an RTD is not a monotonic function of the incident particle energy. Rather, it is oscillatory and admits narrow peaks of total or almost total transmission well below the cutoff energy for classical transmission. By changing the bias voltage of an external electrostatic potential applied to the system, the resonance may be tuned to admit electrons of varying energies.

We shall assume that the electron trajectory is ballistic. In the quantum region, this simplification is appropriate since the electron mean free path is substantially larger than the barrier thickness. However, away from the barrier this simplification is physically unrealistic since the electron mean free path is small compared to the classical length scale for a dense medium. In this case, a relaxation term or collision operator should be added to the Liouville equation to capture the particle dynamics. Since we require that the Hamiltonian be only locally preserved, the model may be extended to a dissipative system, for which the Hamiltonian is continuous, without changing the approach discussed in Section 2.2 and Section 3.1. Hence, for the purpose of validation, the assumption is reasonable.

We construct a representative barrier

$$V(x) = \begin{cases} +\frac{1}{2}V_0 & x \in (-\infty, -a-b] \\ -\frac{1}{2}V_0 x/(a+b) + V_b & x \in (-a-b, -a] \cup (a, a+b] \\ -\frac{1}{2}V_0 x/(a+b) & x \in [-a, a+b] \\ -\frac{1}{2}V_0 & x \in (a+b, \infty) \end{cases}$$

where the external potential bias $V_0 = 0.48$, the thickness of each barrier $b = 0.9\varepsilon$, the thickness of the well separating the barriers $2a = 1.2\varepsilon$, and the height of each barrier $V_b = 2.25$. See Figure 3.6. We take Gaussian initial distributions (3.25) and (3.26) with $\sigma_x = 0.05$, $\sigma_p = 0.15$, $x_0 = -1$ and $p_0 = 1$. The solutions are computed over the domain $[-4, 4]$ and compared at time $t = 2.5$.

The von Neumann equation is solved indirectly using the WKB initial conditions (3.18) with weight distribution (3.19). We use a Crank-Nicolson finite-difference method to solve the Schrödinger equations. To ensure that the weight function is sufficiently resolved, we take $N = (5\varepsilon)^{-1}$ Schrödinger solutions with initial values equally spaced over $8\sigma_p$ about p_0.

The semiclassical Liouville solution is solved using the numerical method proposed in Section 3.1 using an N grid points over $[-4, 4]$ in x, $2N$ grid points over $[-3, 3]$ in p and $3N$ steps in time. The exact solution is computed using equation (3.22) with transmission and reflection probabilities calculated using the transfer matrix method. In computing the transfer matrix for both the numerical and exact solutions, the quantum barrier is discretized using 2000 grid point over the length 6ε for an arbitrary ε. The results are shown in Figure 3.7 and Table 3.5. We calculate an l^1-convergence rate of 1.7 in $\Delta x, \Delta p, \Delta t$.

3.5. Errors in solutions of Example 3.2.4 for various mesh sizes Δx.

grid points	80	160	320	640
l^1-error	3.01×10^{-1}	1.37×10^{-1}	4.43×10^{-2}	8.90×10^{-3}

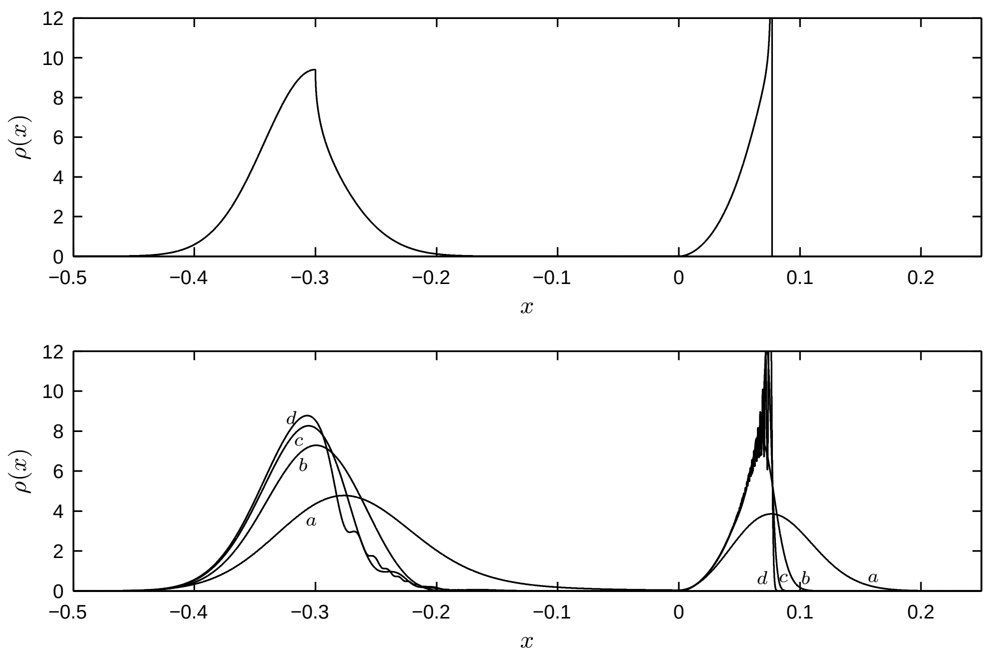

FIGURE 3.2. Position densities for the semiclassical Liouville (top) and Schrödinger (bottom) solutions of Example 3.2.1. The Schrödinger solution shows $\varepsilon =$ (a) 200^{-1}, (b) 800^{-1}, (c) 3200^{-1} and (d) 12800^{-1}. The position density of Liouville solution exhibits a caustic near $x = 0.08$ and the peak is unbounded. For the Schrödinger solution the peak reaches a height of 19 for the $\varepsilon = 12800^{-1}$.

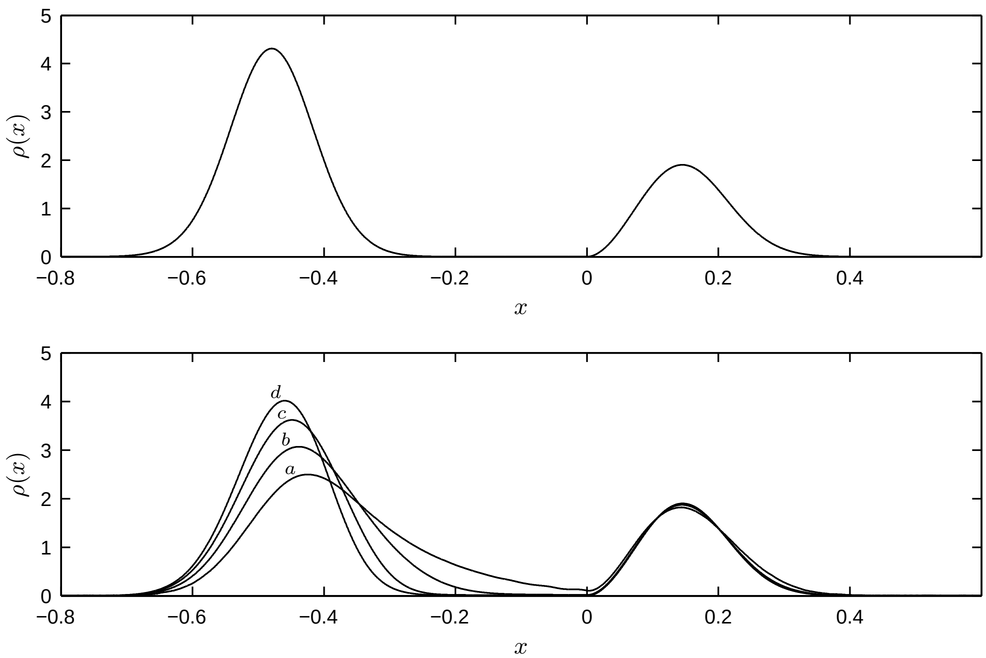

FIGURE 3.3. Position densities for the semiclassical Liouville (top) and von Neumann (bottom) solutions of Example 3.2.2. The von Neumann plot shows ε equal to (a) 64^{-1}, (b) 128^{-1}, (c) 256^{-1} and (d) 512^{-1}.

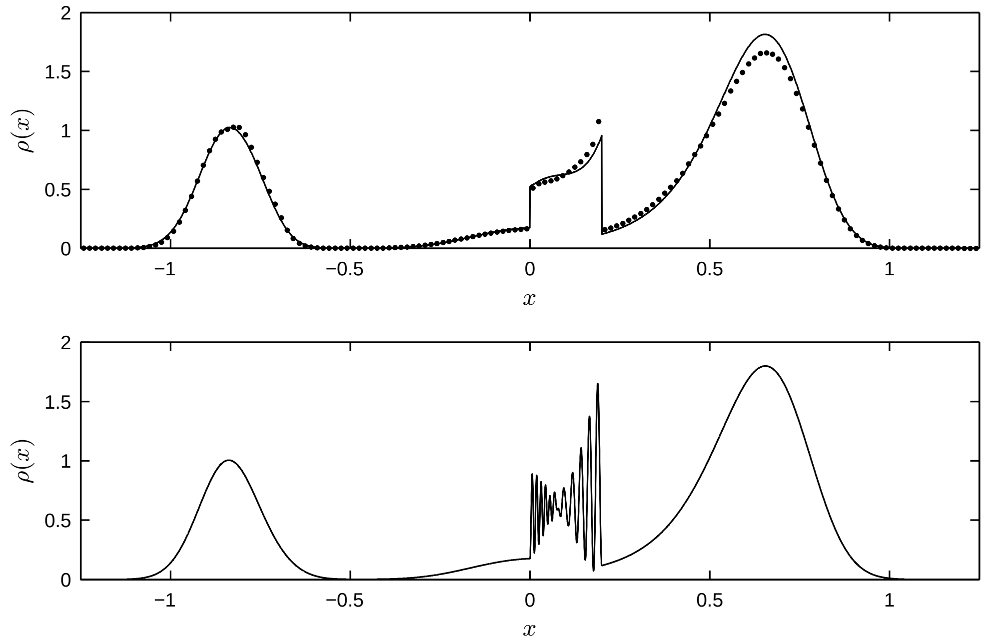

FIGURE 3.4. Position densities for the numerical semiclassical Liouville (top) and von Neumann (bottom) solutions of Example 3.2.3. The • in the Liouville plot shows the numerical solution for with 150 grid points over the domain $[-1.25, 1.25]$. The solid line shows the numerical solution for 3200 grid points. The von Neumann solution is for $\varepsilon = 0.002$.

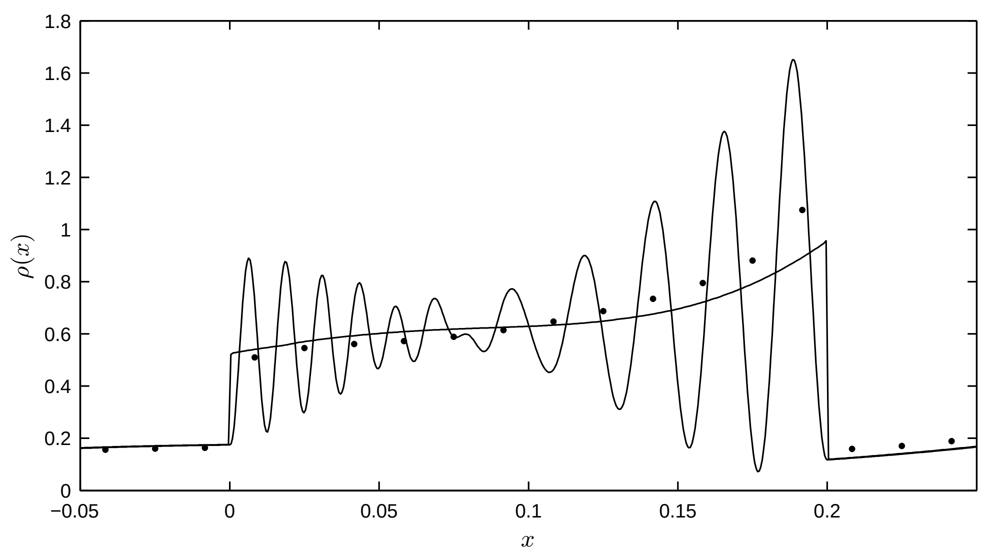

FIGURE 3.5. Detail of Figure 3.4 showing position densities for the numerical semiclassical Liouville and von Neumann solutions. The • shows the numerical solution for with 150 grid points over the domain $[-1.25, 1.25]$. The solid line shows the "exact" Liouville solution and the von Neumann solution using $\varepsilon = 0.002$.

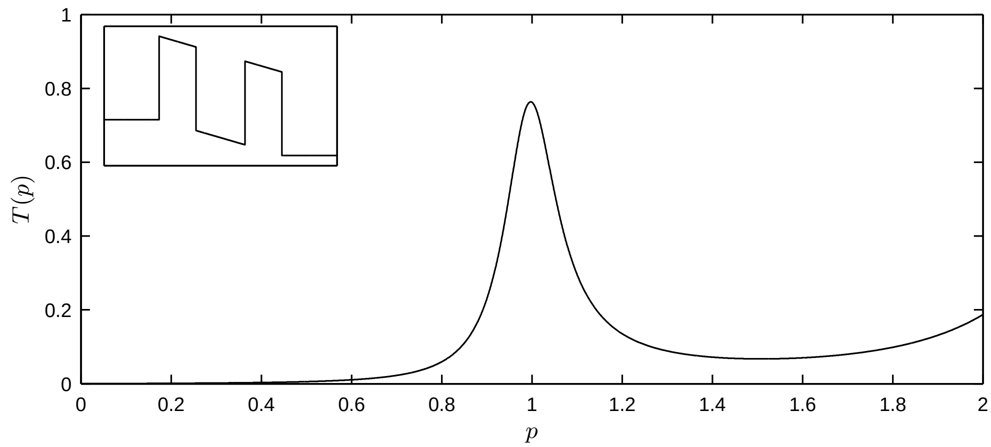

FIGURE 3.6. Transmission probability as a function of the momentum p for the RTD barrier—shown in the inset—presented in Example 3.2.4.

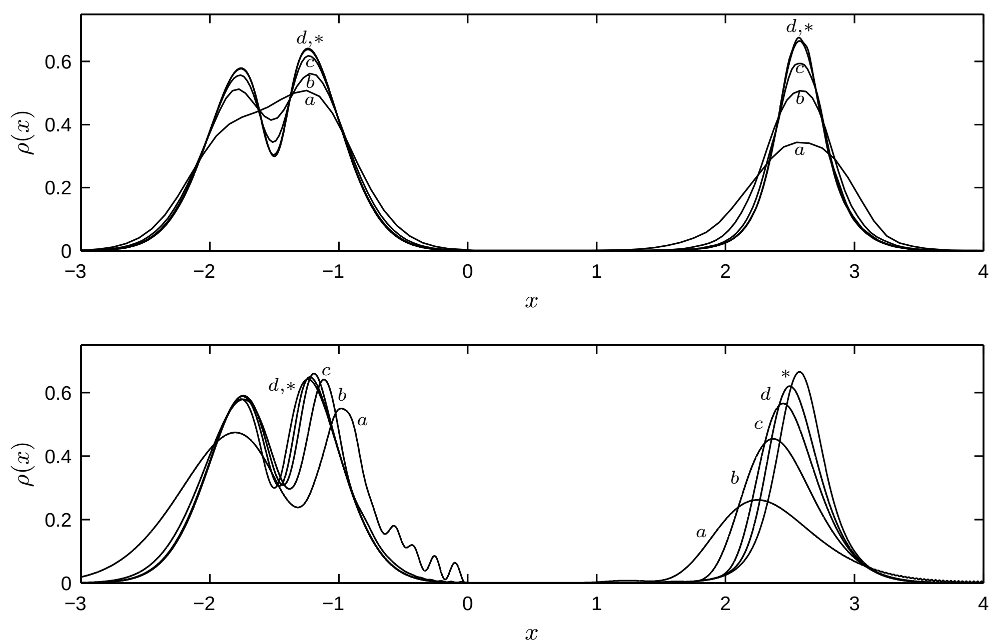

FIGURE 3.7. Position densities for the numerical semiclassical Liouville (top) and von Neumann (bottom) solutions of Example 3.2.4. The Liouville solution shows the numerical solution for (a) 80, (b) 160,(c) 320 and (d) 640 grid points. The von Neumann solution is plotted for $\varepsilon =$ (a) 50^{-1}, (b) 100^{-1}, (c) 200^{-1} and (d) 400^{-1}. The exact solution $(*)$ is also plotted in each case.

Chapter 4

Semiclassical Model and Numerical Method in Two Dimensions

4.1 Extension to multiple dimensions

Multiple dimensions presents several challenges to computing both the quantum von Neumann equation and the semiclassical limit. Not only do the algorithms become more complicated as more variables must be taken into account but also limitations in computer resources (computing time and memory) introduce unavoidable obstacles. Such obstacles are the primary motivation for the development of a computationally efficient and tractable semiclassical model. The von Neumann model for d-dimensional dynamics requires a $2d$-dimensional density matrix. Whereas one may need 15MB of computer memory to compute one-dimensional dynamics over a unit interval with the $\varepsilon = 500^{-1}$ using a direct method, one would need 15TB of computer memory to compute the equivalent two-dimensional dynamics using the same method. Aside from memory, a two-dimensional solution needs a million times as many floating point operations as the equivalent one-dimensional solution. While an indirect method of solution mitigates the memory concern by solving a large number of d-dimensional Schrödinger equations independently, such an approach is impractical for general initial distributions.

The so-called "curse of dimensionality" also afflicts the numerical solution to the semiclassical model. One could solve most one-dimensional problems with a typical computer using a dense, concurrent finite volume approach. In higher dimensions, such an approach in general is simply not effective. Consider the solution to a two-dimensional problem, which requires four dimensions in phase space. Even a rather coarse mesh using an array of 100^4 floating-point numbers requires 380MB of memory. Since we also require an additional "swap" array, we find that 100^4 is a practical limit for brute calculation. Because a typical problem requires at least 100 grid-points over a unit interval to resolve details (see Figure 3.7), the finite-volume method developed in Section 3.1.2 is ineffective for general multi-dimensional semiclassical problems. A sparse matrix algorithm may alleviate some of the difficulty; however, such an approach is viable only when the density information is sufficiently local (such as a front), which is typically an exception for von Neumann solutions. In addition, sparse matrices introduce numerical record-keeping issues further reducing the numerical efficiency of the approach.

Instead, we consider a mesh-free, particle method as an effective alternative. For non-interacting particles, the bicharacteristic solutions may be computed independently thereby eliminating the memory constraints. While a finite-volume approach requires a concurrent solution using a dense array, a particle method algorithm may be easily adapted for parallel computation on a distributed computer cluster reducing the simulation run time. Furthermore, because other related physical models, such as for plasmas, often rely on particle methods for simulation it is quite natural to use such an approach for thin quantum barriers.

While mitigating one set of challenges, the particle method introduces another set. Since we use the bicharacteristics to track information directly, divergence of the bicharacteristics is problematic for all but trivial examples. Because of this one must periodically reconstruct of the data. Furthermore, reconstruction of the data is difficult in regions where the particles are sparse and smoothing techniques may required to mollify the numerical solution.

Formally, we define a particle as the approximation to a Dirac measure using some type of cutoff function [37]. The particle method consists of first approximating the initial conditions $f_0(r) = \int f_0(r)\delta(r - \tilde{r})\, d\tilde{r}$ by a linear combination of Dirac measures $f_0^h = \sum_{j=1}^{N} w_j \delta(r - r_j)$ for some set $\{r_j, w_j\}$ with position $r_j \in \mathbb{R}^d \times \mathbb{R}^d$ and weight $w_j \geq 0$ where N is the sample size. The set $\{r_j, w_j\}$ may be chosen by either a Monte Carlo method or a deterministic method. In a Monte Carlo method, one samples r_j randomly from a distribution and sets $w_j = N^{-1} \int f_0(r)\, dr$. In a deterministic approach, one assigns r_j based on a uniform or nonuniform mesh and sets $w_j = \int_{C_j} f_0(r)\, dr$ for a cell $C_j \in \mathbb{R}^d \times \mathbb{R}^d$. A problem is solved by considering the time evolution of these particles with the appropriate weights. To solve the Liouville equation, where $\delta(x(t) - \tilde{x})\delta(p(t) - \tilde{p})$ defines a single bicharacteristic for the Hamiltonian $H(\tilde{x}, \tilde{p})$, we solve the Hamiltonian system of equations (2.1) for each particle sampled from $f_0(x, p)$.

The focus of this chapter is to develop an efficient numerical discretization of the semiclassical model presented in Section 2.2 in two dimensions. Although we limit the discussion to two-dimensional physical space, the extension three dimensions follows using a similar treatment. As in the one-dimensional case, we use the simplifying assumptions that the effective width of a thin quantum barrier is $O(\varepsilon)$, the distance between neighboring barriers is $O(1)$, and the gradient in the the potential is $O(1)$ except at quantum barriers. Furthermore, we require that coherence time be sufficiently short so that we may neglect interference away from the barrier. In two-dimensional space, we consider the quantum barrier as a smooth one-dimensional curve $\Gamma_{\mathcal{Q}}$ separating two classical regions $\mathcal{C}_1$ and $\mathcal{C}_2$. In addition to changing across the width of the barrier, the potential may also change along the length of the barrier at either the classical $O(1)$ length scale or a quantum $O(\varepsilon)$ length scale. Hence, in the semiclassical limit not only is the potential discontinuous at the barrier in a direction normal to the barrier curve, but the potential may also be discontinuous along the barrier curve. As in the one-dimensional case, we prescribe an interface condition to match local solutions in order to construct the global bicharacteristic solution. But unlike the interface condition for one-dimensional dynamics that combines just two bicharacteristics, the interface condition for two-dimensional dynamics, potentially joins a continuum of bicharacterist computed using the time-independent Schrödinger equation.

4.2 A semiclassical approach and numerical discretization

4.2.1 A semiclassical approach

Whereas in one dimension for which there are only two momenta associated with a Hamiltonian E (namely $+p$ and $-p$), in two dimensions there are a continuum of momenta $\mathbf{p}(\theta) = (p\cos\theta, p\sin\theta)$. Along a local bicharacteristic the momentum of a particle is uniquely determined by continuity of the potential. But across a quantum barrier, where potential is discontinuous and the gradient of the potential is classically undefined, the continuation of the momenta is not unique. In order to match bicharacteristics, we use information at the quantum scale to construct an interface condition.

The two-dimensional analogues to the pull interface condition (2.16) and the push interface condition (2.17) are

$$f(\mathbf{x}_{\text{out}}, p_{\text{out}}, \theta_{\text{out}}) = \int_{-\pi/2}^{\pi/2} R(\theta; p_{\text{in}}, \theta_{\text{out}}) f(\mathbf{x}_{\text{in}}, p_{\text{in}}, \theta)\, d\theta + \int_{-\pi/2}^{\pi/2} T(\theta; q_{\text{in}}, \theta_{\text{out}}) f(\mathbf{x}_{\text{in}}, q_{\text{in}}, \theta)\, d\theta \quad (4.1)$$

and

$$f(\mathbf{x}_{\text{in}}, p_{\text{in}}, \theta_{\text{in}}) = \int_{-\pi/2}^{\pi/2} R(\theta; p_{\text{out}}, \theta_{\text{in}}) f(\mathbf{x}_{\text{out}}, p_{\text{out}}, \theta)\, d\theta + \int_{-\pi/2}^{\pi/2} T(\theta; q_{\text{out}}, \theta_{\text{in}}) f(\mathbf{x}_{\text{out}}, q_{\text{out}}, \theta)\, d\theta \quad (4.2)$$

respectively. Here, $R(\theta_{\text{out}}; p_{\text{in}}, \theta_{\text{in}})$ is the probability of a particle incident with momentum p_{in} at an incident angle θ_{in} being reflected at a reflection angle θ_{out}, $T(\theta_{\text{out}}; p_{\text{in}}, \theta_{\text{in}})$ is the probability of a particle incident with momentum p_{in} at incident angle θ_{in} being transmitted at a refraction angle θ_{out}, and $q^2 = p^2 - 2m\Delta V$.

Where the potential is discontinuous, one may treat the gradient of the potential as an impulse force. However, the direction of such a force may not be well-defined at the classical scale. If the potential is discontinuous both in the direction normal to the barrier and also along the length of the barrier, we must use the solution at the quantum scale to determine the appropriate scattering angles. We shall refine this idea when we discuss the quantum scale solution in Section 4.2.2. If the semiclassical potential $V(x, y)$ is discontinuous in the direction normal to the quantum barrier curve Γ_Q but is continuous along the length of Γ_Q, we take the impulse force normal to the barrier curve. In this case, one has as a consequence of conservation of the Hamiltonian that the change in momentum for a reflected particle is

$$\Delta \mathbf{p} = -2(\mathbf{p}_{\text{in}} \cdot \hat{n})\hat{n} \tag{4.3}$$

where $\hat{n}$ is the unit normal to the barrier $\mathbf{p}_{\text{in}}$ denotes the incident momentum; and for a transmitted particle, the change in momentum is

$$\Delta \mathbf{p} = (\sqrt{|\mathbf{p}_{\text{in}} \cdot \hat{n}|^2 + 2m\Delta V} - \mathbf{p}_{\text{in}} \cdot \hat{n})\hat{n}. \tag{4.4}$$

One may relate the angle of refraction to the angle of incidence (defined with respect to the unit normal) by using the conservation of the Hamiltonian to derive an expression analogous to Snell's law of geometric optics

$$\sin\theta_2 = \sin\theta_1 / \sqrt{1 + 2m(V_1 - V_2)/|\mathbf{p}|^2}$$

where θ_1 is the angle of incidence, θ_2 is the angle of refraction, V_1 is the potential on the incident side and V_2 is the potential on the scattered side. From this expression, one may note that when the angle of incidence is greater (shallower) than a critical angle

$$\theta_1 > \theta_c \equiv \cos^{-1}\left(\sqrt{2m(V_2 - V_1)/|\mathbf{p}|^2}\right) \tag{4.5}$$

the particle is totally reflected by the barrier.

In the following sections, we present the particle method which solves the semiclassical Liouville equation. As in the one-dimensional case, the algorithm consists of an initialization routine and a Liouville solver. During initialization, we determine transmission and reflection coefficients as a function of the incident momentum along the interface from both sides. Calculation of transmission and reflection coefficients for a two-dimensional interface is an extension of calculation of those coefficients in the one-dimensional case. As in one dimension, we solve the problem by computing the stationary solution to the time-independent Schrödinger equation. For the semiclassical model, we consider the quantum barrier as a curve $\Gamma_{\mathcal{Q}}$ separating two classical regions $\mathcal{C}_1$ and $\mathcal{C}_2$. Because the potential may change along the length of the curve, we compute the transmission and reflection coefficients locally at each point along the curve. Consider a point $(x_0, y_0) \in \Gamma_{\mathcal{Q}}$ and define the local coordinates (x, y) where the x-direction is normal to $\Gamma_{\mathcal{Q}}$ the barrier at (x_0, y_0) and the y-direction is parallel to $\Gamma_{\mathcal{Q}}$ at (x_0, y_0). By assumption, the width of the quantum barrier is $O(\varepsilon)$ in the x-direction and the length of the quantum barrier is $O(1)$ in the y-direction. Formally, we will associate the semiclassical quantum barrier $\Gamma_{\mathcal{Q}}$ with a region $\mathcal{Q}$ bordered by the classical regions $\mathcal{C}_1$ and $\mathcal{C}_2$. By assumption the gradient of the potential $V(x, y)$ in classical regions is $O(1)$.

Consider the two-dimensional time-independent Schrödinger equation

$$-\frac{\varepsilon^2}{2m}\left(\frac{\partial^2}{\partial x^2} + \frac{\partial^2}{\partial y^2}\right)\psi^\varepsilon(x, y) + V^\varepsilon(x, y)\psi^\varepsilon(x, y) = E\psi^\varepsilon(x, y). \tag{4.6}$$

By rescaling x and y by ε ($\tilde{x} = \varepsilon x$ and $\tilde{y} = \varepsilon y$), the Schrödinger equation (4.6) may locally be expressed as

$$-\frac{1}{2m}\left(\frac{\partial^2}{\partial \tilde{x}^2} + \frac{\partial^2}{\partial \tilde{y}^2}\right)\psi(\tilde{x}, \tilde{y}) + V(\tilde{x}, \tilde{y})\psi(\tilde{x}, \tilde{y}) = E\psi(\tilde{x}, \tilde{y}). \tag{4.7}$$

By letting $\varepsilon \to 0$, we may regard $\mathcal{C}_1$ and $\mathcal{C}_2$ as the semiinfinite regions $\mathcal{C}_1 = \{\ (x, y) \mid x < x_1\ \}$ and $\mathcal{C}_2 = \{\ (x, y) \mid x > x_2\ \}$ separated by an infinite strip $\mathcal{Q} = \{\ (x, y) \mid x_1 \leq x \leq x_2\ \}$ for some x_1 and x_2. We solve the time-independent Schrödinger equation over $\mathcal{Q}$ using information in $\mathcal{C}_1$ and $\mathcal{C}_2$ to generate transmission and reflection coefficients. We are interested in computing the transmission and reflection coefficients locally, so variations in the potential that are on the classical $O(1)$ lengthscale in the y-direction may be neglected at the quantum $O(\varepsilon)$ lengthscale. Hence, we define

$$V(x, y) = \begin{cases} V_1, & (x, y) \in \mathcal{C}_1 \\ V_{\mathcal{Q}}(x, y), & (x, y) \in \mathcal{Q} \\ V_2, & (x, y) \in \mathcal{C}_2 \end{cases} \tag{4.8}$$

where V_1 and V_2 are constants.

4.2.2 Routine initialization

In this section we discuss the quantum transmitting boundary (QTB) method [7, 28] as a means of determining the reflection and transmission coefficients of the thin two-dimensional quantum barrier. The QTB method is used to solve the time-independent Schrödinger equation in a region with open boundary conditions. By using continuity of the solution and its derivative at the boundaries of an open quantum system in conjunction with a solution with undetermined coefficients in the exterior region, one formulates a boundary value problem for the interior region. The unknown coefficients are eliminated from the problem by combining the Dirichlet boundary conditions with the Neumann boundary conditions to get mixed boundary conditions. Once the solution in the interior is known, it may be used on boundaries to recover the unknown coefficients. The approach differs from the transfer matrix method in that the QTB method first solves the Schrödinger equation numerically in the quantum region as a means of deriving the scattering coefficients. The transfer matrix method, on the other hand, uses the exact solution to the Schrödinger equation over several smaller regions as a means of connecting boundary values. While the transfer matrix method is accurate over a wider range of momenta, the QTB has a natural extension to two or more dimensions. Approaches to compute the solution to the time-independent Schrödinger equation using transfer-matrix methods for two-dimensional geometries are discussed in [10, 39].

We adapt the approach proposed by Lent and Kirkner [28]. Consider the solution to the local time-independent Schrödinger equation (4.7). Here, and in the sequel, the tildes on x and y are dropped in order to simplify notation. Without loss of generality, we take the potential in region $\mathcal{C}_1$ to be zero ($V_1 \equiv 0$). In this case, $E = p_1^2/2m = p_2^2/2m + V_2$ where p_1 is the magnitude of the momentum of a particle in region $\mathcal{C}_1$ and p_2 is the magnitude of the momentum of a particle in region $\mathcal{C}_2$.

The solution to the local Schrödinger equation (4.7) may be written as the piecewise function

$$\psi(x,y) = \begin{cases} \psi_1(x,y), & (x,y) \in \mathcal{C}_1 \\ \psi_{\mathcal{Q}}(x,y), & (x,y) \in \mathcal{Q} \\ \psi_2(x,y), & (x,y) \in \mathcal{C}_2 \end{cases}$$

for which the components $\psi_1(x,y)$, $\psi_{\mathcal{Q}}(x,y)$ and $\psi_2(x,y)$ are related by appropriate matching conditions. In regions $\mathcal{C}_1$ and $\mathcal{C}_2$, where the potential $V(x,y)$ is constant, the Schrödinger equation simplifies to the Helmholtz equations

$$-\Delta\psi_j(x,y) = p_j^2\psi_j(x,y), \qquad j = 1,2 \tag{4.9}$$

which have the general solutions

$$\psi_j(x,y) = \int_{-\pi}^{\pi} a_j(\theta) e^{ip_j(x\cos\theta + y\sin\theta)}\,d\theta, \qquad j = 1,2. \tag{4.10}$$

The current density as discussed in Section 3.1.1 is defined as $J(x,y) = m^{-1}\mathrm{Im}\,\left(\overline{\psi}(x,y)\nabla\psi(x,y)\right)$ where m is the effective mass. For

$$\psi(x,y) = \int_{-\pi}^{\pi} a(\theta) e^{ip(x\cos\theta + y\sin\theta)}\,d\theta$$

we have

$$\begin{aligned}\overline{\psi}(x,y)\nabla\psi(x,y) &= ip\int_{-\pi}^{\pi} \overline{a}(\theta)e^{-ip(x\cos\theta+y\sin\theta)}\,d\theta \int_{-\pi}^{\pi}(\cos\theta,\sin\theta)a(\theta)e^{ip(x\cos\theta+y\sin\theta)}\,d\theta \\ &= ip\int_{-\pi}^{\pi}\int_{-\pi}^{\pi}\overline{a}(\theta_1)a(\theta_2)(\cos\theta_2,\sin\theta_2)e^{-ip(x(\cos\theta_1-\cos\theta_2)+y(\sin\theta_1-\sin\theta_2))}\,d\theta_1\,d\theta_2.\end{aligned}$$

To determine transmission and reflection coefficients, we need the average directional flux at the barrier. Integrating this over y we have

$$\begin{aligned}&\int_{-\infty}^{\infty}\overline{\psi}(x,y)\nabla\psi(x,y)\,dy \\ &\quad= ip\int_{-\pi}^{\pi}\int_{-\pi}^{\pi}\int_{-\infty}^{\infty}\overline{a}(\theta_1)a(\theta_2)(\cos\theta_2,\sin\theta_2)e^{-ipx(\cos\theta_1-\cos\theta_2)}e^{-ipy(\sin\theta_1-\sin\theta_2)}\,dy\,d\theta_1\,d\theta_2 \\ &\quad= ip\int_{-\pi}^{\pi}\int_{-\pi}^{\pi}\overline{a}(\theta_1)a(\theta_2)(\cos\theta_2,\sin\theta_2)e^{-ipx(\cos\theta_1-\cos\theta_2)}\delta(\theta_1-\theta_2)\,d\theta_1\,d\theta_2 \\ &\quad= ip\int_{-\pi}^{\pi}|a(\theta)|^2(\cos\theta,\sin\theta)\,d\theta\end{aligned}$$

Hence, the directional contribution to average current density along the y-axis is

$$J_j(x,y,\theta) = |a_j(\theta)|^2 p_j(\cos\theta,\sin\theta) \qquad j = 1,2 \tag{4.11}$$

which says that the magnitude of the particle flux through a point in region $\mathcal{C}_1$ at an angle θ is $p_1|a_1(\theta)|^2$ and the magnitude of the particle flux through a point in region $\mathcal{C}_2$ at an angle θ is $p_2|a_2(\theta)|^2$.

Consider particle initially in region $\mathcal{C}_1$ that strikes the barrier from the left with momentum p_1 at an angle of incidence θ_{in}. The particle scatters with momentum p_1 into region $\mathcal{C}_1$ if reflected and momentum p_2 into region $\mathcal{C}_2$ if transmitted. In this case, the solutions to equations (4.9) are

$$\psi_1(x,y) = e^{ip_1((x-x_1)\cos\theta_{\text{in}}+y\sin\theta_{\text{in}})} + \int_{-\pi/2}^{\pi/2} r(\theta)e^{-ip_1((x-x_1)\cos\theta+y\sin\theta)}\,d\theta \tag{4.12a}$$

$$\psi_2(x,y) = \int_{-\pi/2}^{\pi/2} t(\theta)e^{ip_2((x-x_2)\cos\theta+y\sin\theta)}\,d\theta. \tag{4.12b}$$

where $r(\theta)$ and $t(\theta)$ are some yet unknown scattering distributions. The probability that a particle is scattered at some angle equals the ratio of the scattered current density to the incident current density. From (4.12),

$$p_1(\cos\theta_{\rm in}, \sin\theta_{\rm in}) = \int_{-\pi/2}^{\pi/2} |r(\theta)|^2 p_1(\cos\theta, \sin\theta)\, d\theta + \int_{-\pi/2}^{\pi/2} |t(\theta)|^2 p_2(\cos\theta, \sin\theta)\, d\theta.$$

Hence, the reflection and transmission probability distributions over the sector $(\theta - \frac{1}{2}d\theta, \theta + \frac{1}{2}d\theta)$ for incident $(p_1, \theta_{\rm in})$ are

$$dR(\theta) = |r(\theta)|^2 \frac{\cos\theta}{\cos\theta_{\rm in}} d\theta \quad \text{and} \quad dT(\theta) = |t(\theta)|^2 \frac{p_2\cos\theta}{p_1\cos\theta_{\rm in}} d\theta.$$

While the form of the solutions (4.12) is convenient for discussing scattering solutions, it is inconvenient for actually determining them since the unknows $r(\theta)$ and $t(\theta)$ are coupled through the integrals. The Schrödinger solution in region $\mathcal{Q}$ is a boundary value problem with boundaries parallel to the y-axis. By expressing the solutions (4.12) in terms of the y-components of the momenta, we may rewrite them in the equivalent forms

$$\psi_1(x, y) = e^{i\eta_1(\xi_{\rm in})(x-x_1)} e^{i\xi_{\rm in} y} + \int_{-\infty}^{\infty} s_1(\xi) e^{-i\eta_1(\xi)(x-x_1)} e^{i\xi y}\, d\xi, \qquad \text{with } \xi = p_1 \sin\theta \tag{4.13a}$$

$$\psi_2(x, y) = \int_{-\infty}^{\infty} s_2(\xi) e^{i\eta_2(\xi)(x-x_2)} e^{i\xi y}\, d\xi, \qquad \text{with } \xi = p_2 \sin\theta \tag{4.13b}$$

where the x-components of the momenta are

$$\eta_1(\xi) = \sqrt{p_1^2 - \xi^2} \quad \text{and} \quad \eta_2(\xi) = \sqrt{p_2^2 - \xi^2};$$

the complex scattering coefficients are

$$s_1(\xi) = \begin{cases} r(\theta) p_1 \cos\theta, & \text{if } |\xi| \le p_1 \\ 0, & \text{otherwise} \end{cases} \quad \text{and} \quad s_2(\xi) = \begin{cases} t(\theta) p_2 \cos\theta, & \text{if } |\xi| \le p_2 \\ 0, & \text{otherwise;} \end{cases} \tag{4.14}$$

and y-component of momentum of the incident particle is $\xi_{\rm in} = p_1 \sin\theta_{\rm in}$. Note that $r(\theta) = s_1(\xi)\eta_1(\xi)$ and $t(\theta) = s_2(\xi)\eta_2(\xi)$ for $\eta_1(\xi)$ and $\eta_2(\xi)$ real. By taking the Fourier transform of the solutions (4.13) with respect to y we have

$$\hat{\psi}_1(x, \xi) = \delta(\xi - \xi_{\rm in}) e^{i\eta_1(\xi)(x-x_1)} + s_1(\xi) e^{-i\eta_1(\xi)(x-x_1)} \tag{4.15a}$$

$$\hat{\psi}_2(x, \xi) = s_2(\xi) e^{i\eta_2(\xi)(x-x_2)}. \tag{4.15b}$$

The Fourier transform of the Schrödinger equation (4.7) is

$$-\frac{\partial^2}{\partial x^2}\hat{\psi}_{\mathcal{Q}}(x,\xi) - \eta_1^2(\xi)\hat{\psi}_{\mathcal{Q}}(x,\xi) + 2m\int_{-\infty}^{\infty} V_{\mathcal{Q}}(x,y)\psi(x,y)e^{-i\xi y}\,dy = 0. \tag{4.16}$$

where we define

$$\hat{\psi}_{\mathcal{Q}}(x,\xi) = \int_{-\infty}^{\infty} \psi(x,y)e^{-i\xi y}\,dy$$

to be the Fourier transform of $\psi_{\mathcal{Q}}(x,y)$ analogous to our definitions for $\hat{\psi}_1(x,\xi)$ and $\hat{\psi}_2(x,\xi)$.

By requiring that the solution $\psi(x,y)$ and its first derivatives be continuous, we have the matching conditions at $x = x_1$ and $x = x_2$

$$\hat{\psi}_j(x_j,\xi) = \hat{\psi}_{\mathcal{Q}}(x_j,\xi) \quad \text{and} \quad \frac{\partial}{\partial x}\hat{\psi}_j(x_j,\xi) = \frac{\partial}{\partial x}\hat{\psi}_{\mathcal{Q}}(x_j,\xi) \tag{4.17a}$$

for $j = 1, 2$. Applying these matching conditions to equations (4.15) we have

$$\hat{\psi}_{\mathcal{Q}}(x_1,\xi) = \delta(\xi - \xi_{\text{in}}) + s_1(\xi), \qquad \hat{\psi}_{\mathcal{Q}}(x_2,\xi) = s_2(\xi), \tag{4.18a}$$

$$\frac{\partial}{\partial x}\hat{\psi}_{\mathcal{Q}}(x_1,\xi) = i\eta_1(\xi)\delta(\xi - \xi_{\text{in}}) - i\eta_1(\xi)s_1(\xi), \qquad \frac{\partial}{\partial x}\hat{\psi}_{\mathcal{Q}}(x_2,\xi) = i\eta_2(\xi)s_2(\xi). \tag{4.18b}$$

Eliminating the unknowns $s_1(\xi)$ and $s_2(\xi)$ gives the boundary conditions

$$i\eta_1(\xi)\hat{\psi}_{\mathcal{Q}} + \frac{\partial}{\partial x}\hat{\psi}_{\mathcal{Q}} = 2i\eta_1(\xi)\delta(\xi - \xi_{\text{in}}) \qquad \text{at } x = x_1, \tag{4.19a}$$

$$i\eta_2(\xi)\hat{\psi}_{\mathcal{Q}} - \frac{\partial}{\partial x}\hat{\psi}_{\mathcal{Q}} = 0 \qquad \text{at } x = x_2. \tag{4.19b}$$

To recover the scattering distribution, we must solve equation (4.16) with the mixed boundary conditions (4.19). From equations (4.14) and (4.18), it follows that

$$r(\theta; p, \theta_{\text{in}}) = \hat{\psi}_{\mathcal{Q}}(x_1, p\sin\theta) - \mathbf{1}_{\theta=\theta_{\text{in}}} \quad \text{and} \quad t(\theta; p, \theta_{\text{in}}) = \hat{\psi}_{\mathcal{Q}}(x_2, p_2(p)\sin\theta)$$

where the indicator function $\mathbf{1}_{\theta=\theta_{\text{in}}}$ equals 1 if $\theta = \theta_{\text{in}}$ and it equals 0 otherwise.

If the potential $V_{\mathcal{Q}}(x,y)$ is constant along the y-direction, *i.e.*, $V_{\mathcal{Q}}(x,y) \equiv V_{\mathcal{Q}}(x)$, then equation (4.16) simplifies to the separable equation

$$-\frac{\partial^2}{\partial x^2}\hat{\psi}_{\mathcal{Q}} - \eta_1^2(\xi)\hat{\psi}_{\mathcal{Q}} + 2mV_{\mathcal{Q}}(x)\hat{\psi}_{\mathcal{Q}} = 0. \tag{4.20}$$

Since $E_x \equiv \eta^2(\xi)/2m$ is simply the contribution of the x-component of the momentum to the kinetic energy, we have the one-dimensional Schrödinger equation

$$-\frac{1}{2m}\frac{\partial^2}{\partial x^2}\hat{\psi}_{\mathcal{Q}} + V_{\mathcal{Q}}(x)\hat{\psi}_{\mathcal{Q}} = E_x\hat{\psi}_{\mathcal{Q}} \tag{4.21}$$

with boundary conditions (4.19). One may also solve the boundary value problem (4.21) by using the transfer matrix method presented in Section 3.1.1. Note that since the solution is constant in the y-direction, the semiclassical impulse force is normal to the barrier curve.

To solve the boundary value problem (4.16) for general potential $V(x, y)$ one may use an iterative solver

$$Au^{(n+1)} = Bu^{(n)}$$

where u_{ij} is the discretization of $\hat{\psi}_{\mathcal{Q}}(x_i, \xi_j)$, A is the finite difference operator

$$Au_{ij} = -\tfrac{1}{2}(\Delta x)^{-2}\left[u_{i+1,j} - 2u_{ij} + u_{i-1,j}\right] + \eta_1^2(\xi_j)u_{ij} \tag{4.22}$$

and

$$Bu_{ij} = -2m\mathcal{F}V_{ij}\mathcal{F}^{-1}u_{ij}$$

where $\mathcal{F}$ is the discrete Fourier transform with respect to y and $V_{ij} = V(x_i, y_j)$ is the discretization of the potential.

4.2.3 A particle method for the semiclassical Liouville equation

Following initialization, we solve the Liouville equation using the particle method by sampling N particles from an initial distribution, solving Hamilton's equations over a given time interval, and then fitting the data to an appropriate mesh. By linearity of the Liouville equation, the particle method may be implemented for each particle independently, permitting us to speed up computation by using a parallel computer cluster.

A particle is sampled from the initial distribution deterministically, for which we associate a weight

$$w_n = \int_{C_n} f(\mathbf{x}, \mathbf{p})\, d\mathbf{x}\, d\mathbf{p} \tag{4.23}$$

to the particle $(\mathbf{x}^0, \mathbf{p}^0, 0)$, or using Monte Carlo sampling, for which we associate a uniform weight $w_n = N^{-1}$. Monte Carlo sampling is important in higher dimensions because it mollifies the "curse of dimensionality" which afflicts deterministic sampling, restricting it to a rather coarse mesh in higher dimensions. In 6-dimensional phase space ($\mathbb{R}^3 \times \mathbb{R}^3$), a billion particle sample when sampled deterministically allows only 30 grid points in each direction. On the other hand, Monte Carlo sampling is inefficient for nonstandard distributions and the solution is noisy even with a substantial sample size.

At each time step we use a symplectic solver [16] to compute $(\mathbf{x}^{n+1}, \mathbf{p}^{n+1}, t^{n+1})$ where we take $t^n = n\Delta t$. We estimate the updated position of the particle

$$\mathbf{x}^* = \mathbf{x}^n + \Delta t \mathbf{p}^n - \tfrac{1}{2}(\Delta t)^2 \nabla V(\mathbf{x}^n) \tag{4.24a}$$

$$\mathbf{p}^* = \mathbf{p}^n - \tfrac{1}{2}\Delta t \left(\nabla V(\mathbf{x}^n) + \nabla V(\mathbf{x}^*)\right). \tag{4.24b}$$

If $\mathbf{x}^*$ is in the same region as $\mathbf{x}^n$, *i.e.,* if the particle has not crossed the barrier $\Gamma_{\mathcal{Q}}$ during the time interval $[t^n, t^{n+1}]$, we let $(\mathbf{x}^{n+1}, \mathbf{p}^{n+1}) = (\mathbf{x}^*, \mathbf{p}^*)$. If $\mathbf{x}^*$ is in a different region from $\mathbf{x}^n$, then we determine the time Δt^* of the barrier crossing

$$\Delta t^* = \left| \frac{d(\mathbf{x}^n)}{d(\mathbf{x}^*) - d(\mathbf{x}^n)} \right| \Delta t \tag{4.25}$$

where $d(x)$ is the signed-distance to the barrier. The time, position and momentum of intersection with the barrier are estimated by the solver (4.24) using Δt^*

We use the push interface condition (4.2) to connect the appropriate bicharacteristics at the barrier. Since the bicharacteristics are not unique, either a Monte Carlo approach or a deterministic branching method must be used to select a bicharacteristic using conditional probabilities based on the incident momentum. In the Monte Carlo method, the scattering angle is chosen by randomly sampling from the distribution of scattering directions. Once an outgoing bicharacteristic is chosen, we compute the position $(\mathbf{x}^{n+1}, \mathbf{p}^{n+1})$ of the particle at time t^{n+1} by using the solver (4.24) with the remaining time step given by $\Delta t - \Delta t^*$ with Δt^* defined by (4.25).

The unit normal vector to $\Gamma_{\mathcal{Q}}$ at $\mathbf{x}^*$ may be calculated either analytically or approximated by using

$$\hat{n} = \nabla d(\mathbf{x}^*)/|\nabla d(\mathbf{x}^*)|$$

where the signed-distance $d(\mathbf{x}^*)$ is interpolated linearly. The component of the momentum normal to $\Gamma_{\mathcal{Q}}$ at $\mathbf{x}^*$ is

$$\mathbf{p}^\perp = (p^\perp, q^\perp) = (\mathbf{p} \cdot \hat{n})\hat{n} = (p_x|\hat{n}_x| + p_y|\hat{n}_y|)(|\hat{n}_x|, |\hat{n}_y|).$$

When the potential $V(x, y)$ is continuous along the length of the barrier curve, there are only two branches—one transmitted branch and one reflected branch. In this case, the correction to the momentum is

$$(\Delta p, \Delta q) = (p^\perp, q^\perp)\left(-1 + \sqrt{1 + 2m\Delta V|\mathbf{p}^\perp|^{-2}}\right) \qquad \text{for transmission,}$$

$$(\Delta p, \Delta q) = -2(|p^\perp|, |q^\perp|) \qquad \text{for reflection.}$$

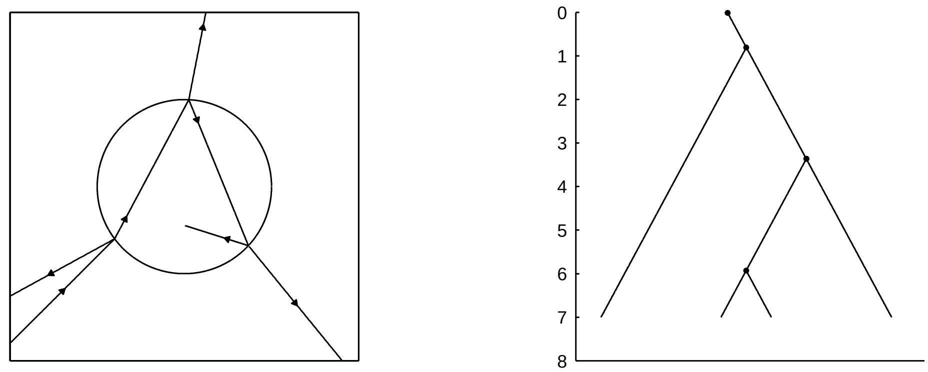

FIGURE 4.1. Phase plane bicharacteristics and the associated binary tree. By considering the solution in terms of a binary tree, one may construct a deterministic solution.

In the case of two branches, it is convenient to use a deterministic branching algorithm by continuing the solution along both transmitted and reflected bicharacteristics. Consider a binary tree with nodes representing the intersections of the bicharacteristic with the barrier. See Figure 4.1. To each branch we associate a conditional scattering (transmission and reflection) probability $s_{k,j}$. We track along a branch using the solver (4.24) until we reach a new node. The particle information $(\mathbf{x}, \mathbf{p}, t)$ is saved at the node and we take the reflection branch. We continue in such a manner—taking the reflection branch at each new node—until the end of the simulation time. The probability that a particle follows the kth forward global bicharacteristic is the product of the conditional probabilities $s_{k,j}$ for each node. Therefore, from equation (2.18) the contribution is

$$w_{n,k} = w_n \prod_{j=1}^{N_k} s_{k,j}. \tag{4.26}$$

We back up to the most recent node that has an unexplored transmission branch. The particle information $(\mathbf{x}, \mathbf{p}, t)$ is set to information previously stored at that specific node. We then take the transmission branch, continuing as above until the end of the simulation. Once all transmission branches have already been explored, *i.e.,* once we have backed up to zeroth node, we have found all the forward bicharacteristics for the particle initially at $(\mathbf{x}^0, \mathbf{p}^0)$.

The solution $\rho(\mathbf{x}, t) = \iint_{-\infty}^{\infty} f(\mathbf{x}, \mathbf{p}, t)\, d\mathbf{p}$ is reconstructed by interpolating over a uniform mesh using a smoothing kernel such as a bicubic spline. Let Δx and Δy denote the mesh spacing and let the nearest mesh point to (x, y) be (x_i, y_j) for some (i, j). Let $r = (x - x_i)/\Delta x$ and $s = (y - y_j)/\Delta y$ denote the offset from that meshpoint. Since we are interested in recovering the position density, we do not need to reconstruct over the momentum. For $l, m \in \{-2, \ldots, 2\}$ define mesh-constrained approximation to (x, y) as

$$\tilde{f}_{i+l,j+m} = w_{n,k}\Lambda(r,l)\Lambda(s,m) \tag{4.27}$$

where

$$\Lambda(r,l) = \sigma(r + l + \tfrac{1}{2}) - \sigma(r + l - \tfrac{1}{2})$$

with the cut-off function [30]

$$\sigma(u) = \begin{cases} 0 & u < -2 \\ \frac{1}{24}(2+u)^4 & -2 < u < -1 \\ \frac{1}{2} + \frac{1}{3}(2u - u^3) - \frac{1}{8}u^4 & -1 < u < 0 \\ \frac{1}{2} + \frac{1}{3}(2u - u^3) + \frac{1}{8}u^4 & 0 < u < 1 \\ 1 - \frac{1}{24}(2+u)^4 & 1 < u < 2 \\ 1 & 2 < u \end{cases}.$$

The deterministic and Monte Carlo particle methods are summarized in algorithms 4.2.3 and 4.2.3 on page 55.

4.3 Numerical Examples

In this section, we present two examples to verify the numerical scheme and validate the semi-classical model. Because of limitations in computer resources required to solve the von Neumann equation, even using an indirect method, we shall limit the analysis to the $O(1)$ Schrödinger wavepacket. In the first example, we consider the scattering on a circular step-potential. This geometry is important because it captures phenomena such as caustics and internal reflection. In the second example, we consider the scattering on an electron diffraction grating for which the potential varies on the quantum length scale along the length of the barrier. Such an interface produces multiple scattering angles.

To solve the time-dependent Schrödinger equation we use a pseudospectral method with Strang splitting similar to the method used for the one-diminsional Schrödinger equation in Section 3.2. The kinetic and potential terms are split so that for each time step we have

$$\psi(x,y,t+\Delta t) = e^{\Delta t B/2}\mathcal{F}^{-1}\left[e^{\Delta t A}\mathcal{F}\left(e^{\Delta t B/2}\psi(x,y,t)\right)\right] \tag{4.28}$$

where

$$A = \exp(\Delta t \frac{\varepsilon}{2mi}(k_x^2 + k_y^2)) \qquad \text{and} \qquad B = \exp(\Delta t \frac{1}{i\varepsilon}V(x,y))$$

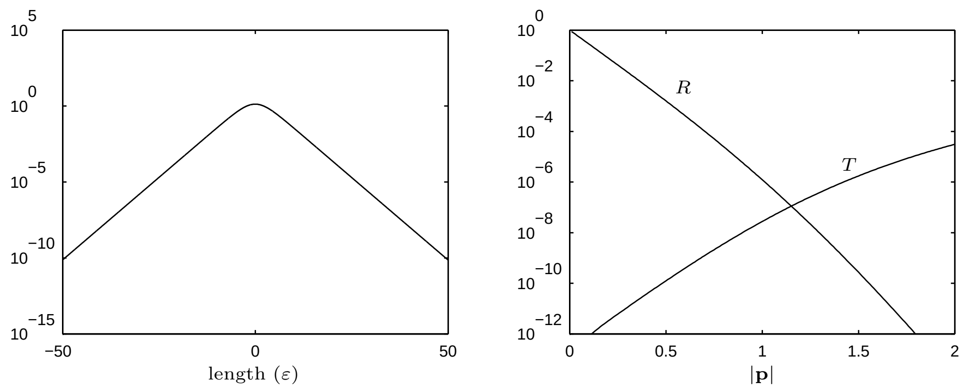

FIGURE 4.2. Reflection (R) and transmission (T) coefficients (left) for the absorbing potential $V(x) = i\frac{9}{8}\text{sech}^2(x/4\varepsilon)$ (right). Note that the potential is "tuned" to absorb the momenta near $p = 1.06$ used in Example 4.3.1.

and the operators $\mathcal{F}$ and $\mathcal{F}^{-1}$ denote the two-dimensional discrete Fourier transform and discrete inverse Fourier transform with respect to the (x, y) and (k_x, k_y) variables. When the potential is discontinuous, the solution exhibits artificial oscillations unless $\Delta t < (\Delta x)^2/\varepsilon$ and $\Delta t < \varepsilon/V(x)$. Because computer memory and computing time constraints in two-dimensional computation, we weaken the conditions that we used in the one-dimensional case and take $\Delta x < \varepsilon/2$, allowing us to take $\Delta t < \varepsilon/4$.

By solving the Schrödinger equation over a periodic domain (rather than an unbounded domain), spurious solutions are eventually introduced as information is transmitted across the domain boundaries. By embedding the domain in a larger domain we can emulate an unbounded domain for a sufficiently short simulation time; however, this approach is inefficient especially in higher dimensions. An alternative method to approximate an unbounded domain is to employ an absorbing potential $V_B(x, y)$ near the boundaries [18, 25]. By adding a negative imaginary potential that decays rapidly away from the domain boundaries, we have the modified Schrödinger equation

$$\frac{\partial}{\partial t}\psi(x, y, t) = \tfrac{1}{2}im^{-1}\Delta\psi(x, y, t) - iV(x, y)\psi(x, y, t) - V_B(x, y)\psi(x, y, t)$$

where $V_B(x, y) > 0$. Such a potential should be strong enough to eliminate (at least to machine precision) any wave information passing through the boundaries, yet not so strong as to reflect the wave. In addition, the potential should be sufficiently narrow so that it does not affect the solution away from the boundary or require an overly large border. In this case, we take

$$V_B(x) = V_0\text{sech}^2((x - x_b)/\varepsilon\ell)$$

where x_b is the position of the domain boundary, V_0 is the barrier strength, and ℓ is the characteristic barrier width. (One may examine other absorbing potentials by using transfer matrices discussed in Section 3.1.1.) For this potential the transmission and reflections coefficients may be found exactly giving [11]

$$T = \left|\frac{\Gamma(-ip\ell-\gamma)\Gamma(-ip\ell+\gamma+1)}{\Gamma(-ip\ell)\Gamma(-ip\ell+1)}\right|^2 \quad \text{and} \quad R = \left|\frac{\Gamma(-ip\ell-\gamma)\Gamma(-ip\ell+\gamma+1)}{\Gamma(-\gamma)\Gamma(\gamma+1)}\right|^2$$

where $\gamma = -\frac{1}{2}+\frac{1}{2}\sqrt{1-8iV_0\ell^2}$ and p is the normal component of the incident momentum. When $p\ell \gg 1$, $\gamma \approx (1-i)V_0^{1/2}\ell$, and hence $T \approx R$ at $p = V_0^{1/2}$. By adjusting V_0 we may "tune" the barrier to absorb a specific range of energies. Note that the reflection and transmission coefficients are independent of ε and by taking $\Delta x = \varepsilon/2$, we may specify the barrier thickness in terms of grid points.

To compare the convergence of the Schrödinger to the semiclassical limit in two dimensions we consider the following L^1-errors:

- the L^1-error of the position probability density function (pdf)

$$\iint_{-\infty}^{\infty} |\rho(x,y,t)-\hat{\rho}(x,y,t)|\, dy\, dx$$

- the L^1-error of the cumulative density function (cdf)

$$\iint_{-\infty}^{\infty} \left|\int_{-\infty}^{x}\int_{-\infty}^{y} \rho(r,s,t)-\hat{\rho}(r,s,t)\, ds\, dr\right| dy\, dx$$

- the L^1-error of the marginal probability distribution function (mpdf)

$$\int_{-\infty}^{\infty} \left|\int_{-\infty}^{\infty} \rho(x,y,t)-\hat{\rho}(x,y,t)\, dy\right| dx$$

- the L^1-error in the cumulative marginal distribution function (mcdf)

$$\int_{-\infty}^{\infty} \left|\int_{-\infty}^{x}\int_{-\infty}^{\infty} \rho(s,y,t)-\hat{\rho}(x,y,t)\, dy\, ds\right| dx.$$

In the above definitions, $\rho(x,y,t) = \iint_{-\infty}^{\infty} f(x,y,p,q,t)\, dp\, dq$ for the semiclassical Liouville solution and $\hat{\rho}(x,y,t) = |\psi(x,y,t)|^2$ for the Schrödinger solution. In both examples we take the effective mass $m = 1$.

4.3.1 Schrödinger $O(1)$ wave envelope with a circular barrier

Consider the circular barrier with unit diameter

$$V(\mathbf{x}) = \begin{cases} 0 & \mathbf{x} \in \Omega_1 \\ \frac{1}{2} & \mathbf{x} \in \Omega_2 \end{cases}$$

where $\Omega_1 = \{ \mathbf{x} \mid |\mathbf{x}| > \frac{1}{2} \}$ and $\Omega_2 = \overline{\Omega}_1^C$. Consider initial conditions

$$\psi(x, y, 0) = \frac{1}{\sqrt{2\pi\sigma^2}} \exp\left(\frac{-(x-x_0)^2 - (y-y_0)^2}{4\sigma^2}\right) \exp\left(\frac{i(p_0 x + q_0 y)}{\varepsilon}\right) \tag{4.29}$$

describing a symmetric Gaussian wavepacket initially located at (x_0, y_0) traveling with momentum (p_0, q_0). In the semiclassical limit we take the initial conditions

$$f(x, y, p, q) = \frac{1}{2\pi\sigma^2} \exp\left(\frac{-(x-x_0)^2 - (y-y_0)^2}{2\sigma^2}\right) \delta(p-p_0)\delta(q-q_0). \tag{4.30}$$

Let $(x_0, y_0) = (-1, -1)$, $(p_0, q_0) = (\frac{3}{4}, \frac{3}{4})$ and $\sigma = \frac{1}{4}$. We compute over a square domain with length $L = 4$. Using equations (3.3) and (3.7), we determine the reflection coefficient to be

$$R(p) = \begin{cases} \left|p - \sqrt{p^2+1}\right|^4 & \text{for a particle entering } \Omega_1 \text{ from } \Omega_2 \\ \left|p - \sqrt{p^2-1}\right|^4 & \text{for a particle entering } \Omega_2 \text{ from } \Omega_1. \end{cases}$$

Also, using equation (4.5) we may determine the critical angle $\theta_c = \cos^{-1}\left(|\mathbf{p}|^{-1}\right)$. For the initial speed $|\mathbf{p}_0| \approx 1.06$, the critical angle $\theta_c \approx 0.34$ and the momenta of the particle in the region Ω_2 is approximately 0.35.

To solve the Schrödinger equation, we use a pseudospectral method with Strang splitting (4.28) with $\Delta x = \varepsilon/2$ and $\Delta t = \varepsilon/4$. To mollify spurious reflections and transmissions across the periodic boundary conditions, we employ an absorbing boundary with width $\ell = 50\varepsilon = 100\Delta x$ encircling the domain. The semiclassical solution is computed using a deterministic particle method with approximately 10^9 particles and reconstructed using a mesh spacing $\Delta x = 100^{-1}$. Since the semiclassical solution is reconstructed over a coarser mesh than the Schrödinger solution, we linear interpolate the semiclassical solution to match the semiclassical and Schrödinger solutions.

The marginal probability (position) density function $\int \rho(x, y, t)\, dy$ for the semiclassical Liouville solution and the Schrödinger solution for several values of ε are shown in Figure 4.3 on page 51. Time evolution of the Schrödinger solutions and semiclassical solutions are shown in Figures 4.4 and 4.5 on pages 56 and 57. The errors in the two solutions are listed in Table 4.1. Based on our study, we find the convergence rate of the l^1-errors to be about first order.

4.1. Errors in solutions of Example 4.3.1 for different values of ε

ε	50^{-1}	100^{-1}	200^{-1}	400^{-1}	convergence
l^1-error (pdf)	4.52×10^{-1}	2.90×10^{-1}	1.73×10^{-1}	1.24×10^{-1}	0.6
l^1-error (cdf)	1.52×10^{-1}	6.01×10^{-2}	3.64×10^{-2}	1.72×10^{-2}	1.0
l^1-error (mpdf)	3.20×10^{-1}	1.01×10^{-1}	5.03×10^{-2}	2.37×10^{-2}	1.2
l^1-error (mcdf)	9.56×10^{-2}	3.08×10^{-2}	1.42×10^{-2}	7.20×10^{-3}	1.2

Notable phenomena emergent in the Schrödinger solution to this example are formation of interior caustics and internal reflection. See Figures 4.4 and 4.5. Suppose a particle originally in a region Ω_1 with potential V_1 is transmitted across an interface Γ_Q near the critical angle and enters a convex region Ω_2 with potential $V_2 > V_1$. The particle "creeps" internally along the interface Γ_Q, and with a nonvanishing probability the particle is trapped in the region of higher potential. While the semiclassical model accurately captures both caustics and internal reflection, the classical model does not.

4.3.2 Electron diffraction grating

Consider the semiclassical potential

$$V(x,y) = \begin{cases} V_{\mathcal{Q}}^0 & \text{if } (x,y) \in \Gamma_{\mathcal{Q}} \\ 0 & \text{otherwise} \end{cases}$$

where $\Gamma_{\mathcal{Q}}$ is the y-axis. Note that $\Gamma_{\mathcal{Q}}$ may be any smooth curve—we take the $\Gamma_{\mathcal{Q}}$ to be y-axis to simplify analysis. The quantum potential $V_{\mathcal{Q}}^0 = \lim_{\varepsilon\to 0} V_{\mathcal{Q}}(\varepsilon x', \varepsilon y')$ where x'-axis is normal to $\Gamma_{\mathcal{Q}}$ and the y'-axis is parallel to the $\Gamma_{\mathcal{Q}}$. Let the local quantum potential (with x and y scaled by ε) be given by

$$V_{\mathcal{Q}}(x,y) = f(x)\,(1+\cos\alpha y) \qquad \text{with} \qquad f(x) = \tfrac{1}{2}(1+\cos\pi x)$$

if $x \in [-1,1]$ and $y \in \mathbb{R}$ where α is some parameter. Take $V(x,y) = 0$ elsewhere.

We begin by determining the scattering coefficients for the barrier. Consider a particle with momentum p (and energy $E = \frac{1}{2}p^2$) with an incident angle θ_{in} and a scattering angle θ. The y-component of the incident momentum is $\xi_{\text{in}} = p\sin\theta_{\text{in}}$ and the y-component of the scattered momentum is $\xi = p\sin\theta$. Then the x-component of the momentum is $\eta(\xi) = \sqrt{p^2-\xi^2}$. Let $\hat{\psi}_{\mathcal{Q}}$

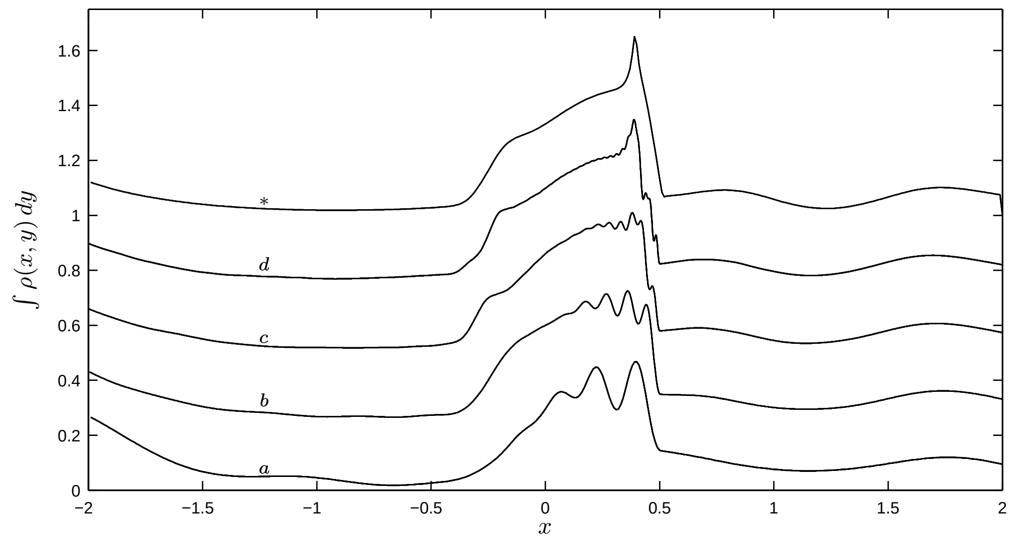

FIGURE 4.3. Marginal position density function for Example 4.3.1 for $\varepsilon =$ (a) 50^{-1}, (b) 100^{-1}, (c) 200^{-1}, (d) 400^{-1} at time $t = 2$. The numerical semiclassical limit is indicated by $*$. The plots are offset by 0.25 for clarity.

be the Fourier transform of $\psi_{\mathcal{Q}}$ with respect to y as defined in Section 4.2.2. By using the identity

$$\int_{-\infty}^{\infty} f(x)(1 + \cos \alpha y)\psi_{\mathcal{Q}}(x, y)e^{-i\xi y}\, dy = \tfrac{1}{2} f(x) \Big(\hat{\psi}_{\mathcal{Q}}(x, \xi + \alpha) + 2\hat{\psi}_{\mathcal{Q}}(x, \xi) + \hat{\psi}_{\mathcal{Q}}(x, \xi - \alpha)\Big)$$

equation (4.16) becomes

$$-\frac{\partial^2}{\partial x^2}\hat{\psi}_{\mathcal{Q}}(x, \xi) - \eta^2(\xi)\hat{\psi}_{\mathcal{Q}}(x, \xi) + f(x) \Big(\hat{\psi}_{\mathcal{Q}}(x, \xi + \alpha) + 2\hat{\psi}_{\mathcal{Q}}(x, \xi) + \hat{\psi}_{\mathcal{Q}}(x, \xi - \alpha)\Big) = 0 \tag{4.31}$$

with the mixed boundary values

$$i\eta(\xi)\hat{\psi}_{\mathcal{Q}} + \frac{\partial}{\partial x}\hat{\psi}_{\mathcal{Q}} = 2i\eta(\xi)\delta(\xi - \xi_{\text{in}}) \qquad \text{at } x = -1 \tag{4.32a}$$

$$i\eta(\xi)\hat{\psi}_{\mathcal{Q}} - \frac{\partial}{\partial x}\hat{\psi}_{\mathcal{Q}} = 0 \qquad \text{at } x = +1. \tag{4.32b}$$

To solve the boundary value problem (4.31) and (4.32) we consider a finite difference method. Let x_i be the discretization of x over $[-1, 1]$ using m grid points with uniform spacing Δx. Let ξ_j be the discretization of ξ using a uniform spacing $\Delta\xi = \alpha/d$ for an integer d. The second-order centered-difference approximation of (4.31) is

$$-\frac{u_{i+1,j} - 2u_{ij} + u_{i-1,j}}{(\Delta x)^2} - \eta_j^2 u_{ij} + (u_{i,j+d} + 2u_{ij} + u_{i,j-d})f_i = 0 \tag{4.33}$$

where we define $u_{ij} = \hat{\psi}_{\mathcal{Q}}(x_i, \xi_j)$, $f_i = f(x_i)$, and $\eta_j = \eta(\xi_j)$. Note the convention that the coefficient i denotes the complex constant i and the subscript i denotes an index. As a simplification, one may restrict ξ_{in} to a gridpoint k ($\xi_{\text{in}} = \xi_k$) and interpolate over the scattering coefficients to approximate intermediate values. The second-order approximation of the boundary conditions (4.32) are

$$i\eta_j u_{1j} + \frac{u_{2,j} - u_{0,j}}{2\Delta x} = 2i\eta_j \delta_{jk} \tag{4.34a}$$

$$i\eta_j u_{mj} - \frac{u_{m+1,j} - u_{m-1,j}}{2\Delta x} = 0. \tag{4.34b}$$

Substituting the value for $u_{0,j}$ from the left boundary condition (4.34a) and substituting the value for $u_{m+1,j}$ from the right boundary condition (4.34b) into equation (4.33), we have the equivalent system of equations

$$\begin{aligned} &\left((\Delta x)^2\eta_j^2 - 2(\Delta x)^2 f_i - 2\right) u_{ij} + u_{i+1,j} + u_{i-1,j} \\ &\qquad - (\Delta x)^2 f_i u_{i,j+d} - (\Delta x)^2 f_i u_{i,j-d} = 0 \text{for} \qquad 1 < i < m \end{aligned} \tag{4.35a}$$

$$\begin{aligned} &2u_{2,j} + \left((\Delta x)^2\eta_j^2 - 2(\Delta x)^2 f_1 - 2 + i2(\Delta x)\eta_j\right) u_{1j} \\ &\qquad - (\Delta x)^2 f_1 u_{1,j+d} - (\Delta x)^2 f_1 u_{1,j-d} = 4i(\Delta x)\eta_j \delta_{jk} \end{aligned} \tag{4.35b}$$

$$\begin{aligned} &2u_{m-1,j} + \left((\Delta x)^2\eta_j^2 - 2(\Delta x)^2 f_m - 2 + i2(\Delta x)\eta_j\right) u_{mj} \\ &\qquad - (\Delta x)^2 f_m u_{m,j+d} - (\Delta x)^2 f_m u_{m,j-d} = 0. \end{aligned} \tag{4.35c}$$

By condition (4.14) we have that $u_{ij} = 0$ if $|\xi_j| \geq p$. Furthermore, the solutions $u_{ij} = 0$ if $j \notin \{\dots, k-d, k, k+d, \dots\}$. Therefore, for each incident momenta ξ_k, we solve system (4.35) for $j \in \{\dots, k-d, k, k+d, \dots\}$. Let $\{J\}$ be the n-element enumeration of this set. In this case, we may express the equations as the system $Mv = b$ where the nm-element vector v is defined using $v_{i+mj} = u_{ij}$, b is defined using $b_{i+mj} = 4i(\Delta x)\eta_j$, and M is the block tridiagonal matrix

$$M = \begin{pmatrix} T^{(1)} & D & & & \\ D & T^{(2)} & D & & \\ & \ddots & \ddots & \ddots & \\ & & D & T^{(n-1)} & D \\ & & & D & T^{(n)} \end{pmatrix}.$$

In this matrix, D are $m \times m$ diagonal matrices with $D_{ij} = -(\Delta x)^2 f_i \delta_{ij}$ and $T^{(J)}$ are $m \times m$ tridiagonal matrices

$$T^{(J)}_{ij} = \left((\Delta x)^2\eta_J^2 - 2(\Delta x)^2 f_i - 2\right)\delta_{ij} + \delta_{i+1,j} + \delta_{i-1,j}$$

with the exceptions $T_{ii}^{(J)} = (\Delta x)^2\eta_J^2 - 2(\Delta x)^2 f_i - 2 + i2(\Delta x)\eta_J$ for $i = 1, m$ and $T_{12}^{(J)} = 2$ and $T_{m,m-1}^{(J)} = 2$.

From (4.11), the transmission coefficients are given by $|v_{m+Jn}|^2\eta_k^{-1}\eta_J$. The reflection coefficients are given by $|1-v_{1+Jn}|^2$ when J corresponds to k incident and $|v_{1+J}|^2\eta_k^{-1}\eta_J$ otherwise. The discrete scattering angles are given by

$$\theta_J = -\sin^{-1}\left(\frac{\xi_k - J\alpha}{|p|}\right)$$

which is simply the Fraunhofer diffraction grating formula

$$J\lambda = d(\sin\theta_{\text{in}} + \sin\theta_J)$$

with wavelength $\lambda = 2\pi\varepsilon/|p|$ and groove spacing $d = 2\pi\alpha^{-1}$.

When n and m are large, we can use a few manipulations to efficiently solve the system $Mv = b$. By moving the top row of M to the bottom (and doing the same for the vector b), we get an equivalent system with an almost upper triangular matrix

$$M' = \begin{pmatrix} D & T^{(2)} & D & & \\ & \ddots & \ddots & \ddots & \\ & & D & T^{(n-1)} & D \\ & & & D & T^{(n)} \\ T^{(1)} & D & & & 0 \end{pmatrix}.$$

To invert such a matrix we rely on the useful Sherman–Morrison–Woodbury algorithm [13]

$$M'^{-1} = (A + UV^T)^{-1} = A^{-1} - A^{-1}U(I + V^T A^{-1}U)^{-1}V^T A^{-1} \tag{4.36}$$

where we take

$$A = \begin{pmatrix} D & T^{(2)} & D & & \\ & \ddots & \ddots & \ddots & \\ & & D & T^{(n-1)} & D \\ & & & D & T^{(n)} \\ & & & & I \end{pmatrix}, \quad U = \begin{pmatrix} 0 \\ \vdots \\ \vdots \\ 0 \\ I \end{pmatrix}, \quad V = \begin{pmatrix} T_1 \\ D \\ 0 \\ \vdots \\ 0 \\ -I \end{pmatrix}.$$

Because A is upper triangular, it is easy and fast to invert by back substitution. The matrix $I + V^T A^{-1}U$ is a dense $m \times m$ matrix that is inverted using LU decomposition. The number of floating-point operations needed to invert M' when n and m are large is $10m^2n + \frac{2}{3}m^3$. The usual block tridiagonal algorithm using the Thomas algorithm requires $\frac{14}{3}m^3n$ floating-point operations because forward-substitution does not preserve the sparsity of the block matrices.

If the incident momentum is $p \leq \frac{1}{2}\alpha$ then $n = 1$ and for each incident bicharacteristic there is one transmitted bicharacteristic and one reflected bicharacteristic. In general, the number of transmitted/reflected bicharacteristics will be

$$N(\xi_{\text{in}}) = 1 + \text{floor}\left[\alpha^{-1}|p - \xi_{\text{in}}|\right] + \text{floor}\left[\alpha^{-1}|p + \xi_{\text{in}}|\right] \leq 2\alpha^{-1}p + 1.$$

To validate the semiclassical model, we took $\alpha = \frac{1}{2}$ and considered the initial conditions (4.29) and (4.29) with $\sigma = 1/16$ and $(p_0, q_0) = (\cos\theta_{\text{in}}, \sin\theta_{\text{in}})$, $(x_0, y_0) = 0.3(-\cos\theta_{\text{in}}, \sin\theta_{\text{in}})$ where $\theta_{\text{in}} = 10°$. The solve the semiclassical model can be solved exactly by considering the method of characteristics and the scattering coefficients computed numerically. In this case

$$\rho(x, y, t) = \rho_0(x^*, y^*) + \sum_k s(\theta_k)\rho_0\left(x^* - \frac{\cos\theta_k - \cos\theta_{\text{in}}}{\cos\theta_k}x, y^* - \frac{\sin\theta_k + \sin\theta_{\text{in}}}{\cos\theta_k}x\right)\mathbf{1}_{(x\cos\theta_k > 0)}$$

where $x^* = x - t\cos\theta_{\text{in}}$ and $y^* = y + t\sin\theta_{\text{in}}$ and $\rho_0(x, y)$ is the position density of the initial distribution (4.29).

The $\rho(x, y) = 2$ contours of the position density for the Schrödinger solution and the semiclassical solution are shown in Figures 4.6 and 4.7 on pages 58 and 59 for $\varepsilon = 200^{-1}$ and 800^{-1}. The errors in the two solutions are listed in Table 4.2. Although the solutions have roughly first-order convergence in probability density functions, the solutions fail to converge in the cumulative density functions. Furthermore, as evident in Figures 4.6 and 4.7, while the semiclassical model does agrees with the Schrödinger solution for small scattering angles, there is a significant discrepancy at larger scattering angles. A possible explanation for this discrepancy is underresolution of the mesh for the Schrödinger solution.

4.2. Errors in solutions of Example 4.3.2 for different values of ε

ε	100^{-1}	200^{-1}	400^{-1}	800^{-1}	convergence
l^1-error (pdf)	6.09×10^{-1}	3.05×10^{-1}	2.25×10^{-1}	2.09×10^{-1}	0.8
l^1-error (cdf)	4.86×10^{-2}	4.82×10^{-2}	5.00×10^{-2}	5.07×10^{-2}	—
l^1-error (mpdf)	3.46×10^{-1}	1.81×10^{-2}	1.33×10^{-1}	1.04×10^{-1}	0.9
l^1-error (mcdf)	6.57×10^{-2}	6.58×10^{-2}	6.82×10^{-2}	6.93×10^{-3}	—

ALGORITHM 4.1. Deterministic semiclassical particle method

0. Initialization. Calculate the transmission/reflection coefficients associated with the components of momentum normal to the interface. Save the coefficients in a table over which to interpolate.

1. Choose a point $(\mathbf{x}^0, \mathbf{p}^0, t^0 = 0)$ and calculate the weight w associated with the initial distribution using (4.23) .

2. While the node index $I > 0$

   (a) Calculate $(\mathbf{x}^*, \mathbf{p}^*)$ from $(\mathbf{x}^n, \mathbf{p}^n)$ using (4.24).

   (b) If $\mathbf{x}^*$ and $\mathbf{x}^n$ are both in the same regions, take $(\mathbf{x}^{n+1}, \mathbf{p}^{n+1}) = (\mathbf{x}^*, \mathbf{p}^*)$. Otherwise:

      i. Compute the position and momentum at barrier $(\mathbf{x}^*, \mathbf{p}^*)$ using (4.25). Compute the unit normal $\hat{n}$ at $\mathbf{x}^*$.

      ii. Increment the node index I and save $(\mathbf{x}^*, \mathbf{p}^*, t^*)$ to the new node.

      iii. Take the reflection branch and calculate $(\mathbf{x}^{n+1}, \mathbf{p}^{n+1})$ using (4.24) with timestep $\Delta t - \Delta t^*$ given by (4.25).

   (c) If $t > t_{\max}$

      i. Reconstruct the solution using (4.27) and (4.26).

      ii. Decrease I to latest node with an unexplored transmission branch.

      iii. Set $(\mathbf{x}^*, \mathbf{p}^*, t^*)$ to value stored at node I.

      iv. Take the transmission branch and calculate $(\mathbf{x}^{n+1}, \mathbf{p}^{n+1})$ using (4.24) with $\Delta t - \Delta t^*$.

ALGORITHM 4.2. Monte Carlo semiclassical particle method

0. Initialization. Calculate the scattering distribution associated with the momentum incident to the quantum barrier. Save the coefficients in a table over which to interpolate.

1. Choose an initial particle $(\mathbf{x}^0, \mathbf{p}^0)$ from the initial distribution using Monte Carlo sampling.

2. For each particle, while $t^n < t^{\max}$

   (a) Calculate $(\mathbf{x}^*, \mathbf{p}^*)$ from $(\mathbf{x}^n, \mathbf{p}^n)$ using (4.24).

   (b) If $\mathbf{x}^*$ and $\mathbf{x}^n$ are both in the same regions, take $(\mathbf{x}^{n+1}, \mathbf{p}^{n+1}) = (\mathbf{x}^*, \mathbf{p}^*)$. Otherwise:

      i. Compute the position and momentum at barrier $(\mathbf{x}^*, \mathbf{p}^*)$ using (4.25) and compute the unit normal $\hat{n}$ at $\mathbf{x}^*$.

      ii. Use Monte Carlo sampling of the scattering coefficient $s(\theta)$ to determine the scattering momentum $\mathbf{p}^*$.

      iii. Calculate $(\mathbf{x}^{n+1}, \mathbf{p}^{n+1})$ using (4.24) with timestep $\Delta t - \Delta t^*$ given by (4.25).

3. Reconstruct the solution using (4.27).

FIGURE 4.4. Solutions for Example 4.3.1 for $\varepsilon = 50^{-1}$ (left) and $\varepsilon = 100^{-1}$ (right) at times $t = 0, 2, 4, 6, 8$.

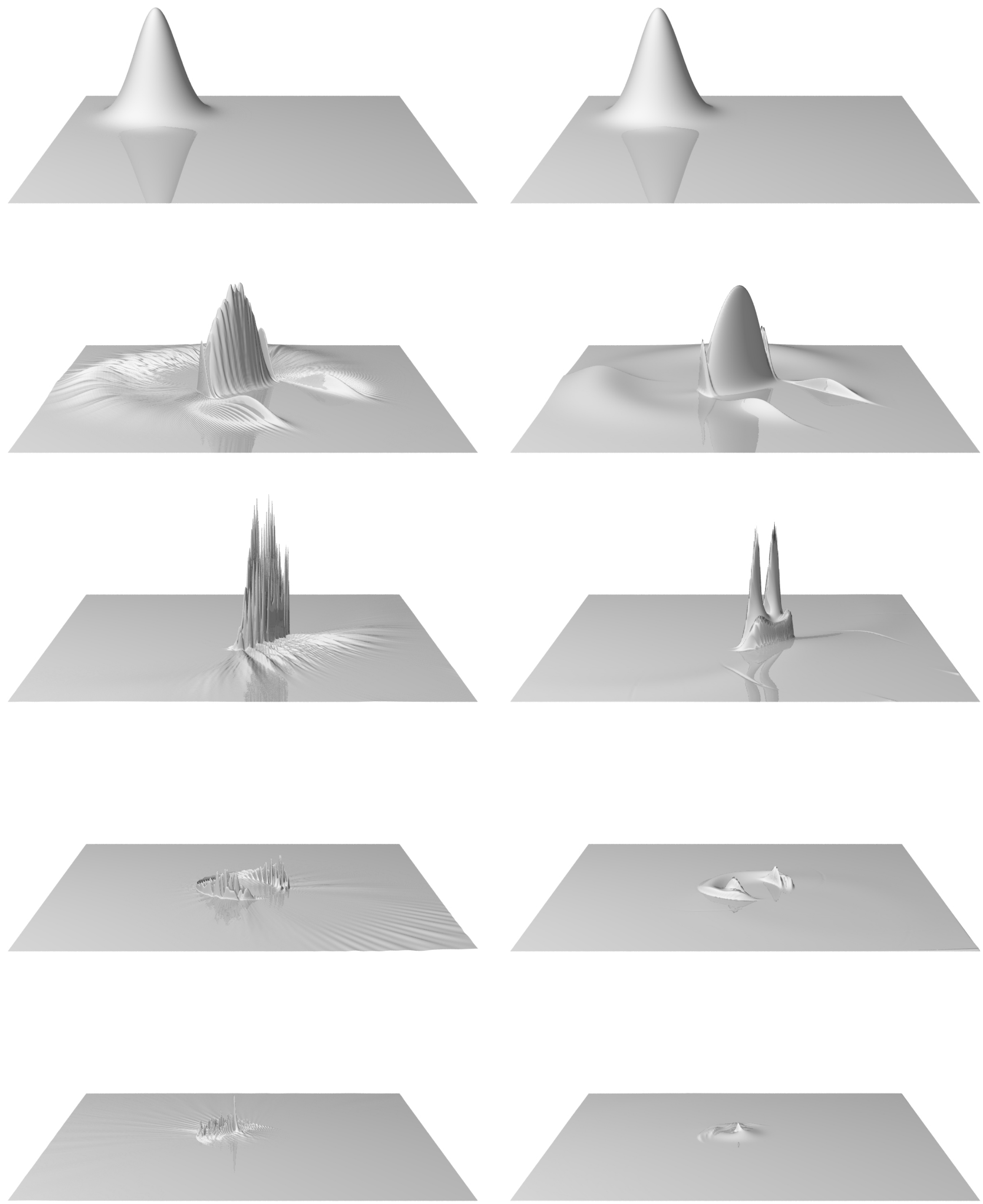

FIGURE 4.5. Solutions for Example 4.3.1 for $\varepsilon = 200^{-1}$ (left) and the semiclassical limit (right) at times $t = 0$, 2, 4, 6, 8.

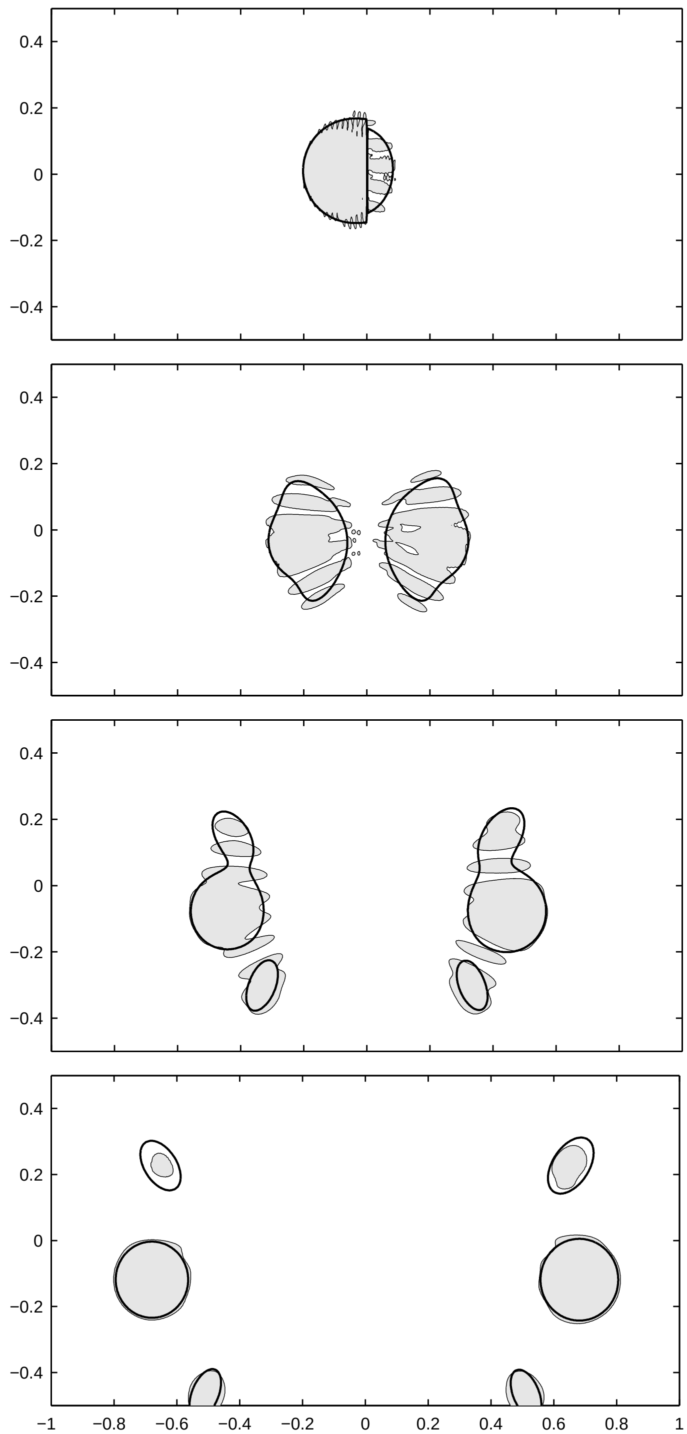

Figure 4.6. Contour plot of solution to Example 4.3.2 at $\rho(x,y) = 2$ for $\varepsilon = 200^{-1}$ at $t = 0.25$, 0.5, 0.75 and 1.0. The contour of the Schrödinger solution is filled in and the contour for numerical semiclassical limit is illustrated by a bold line.

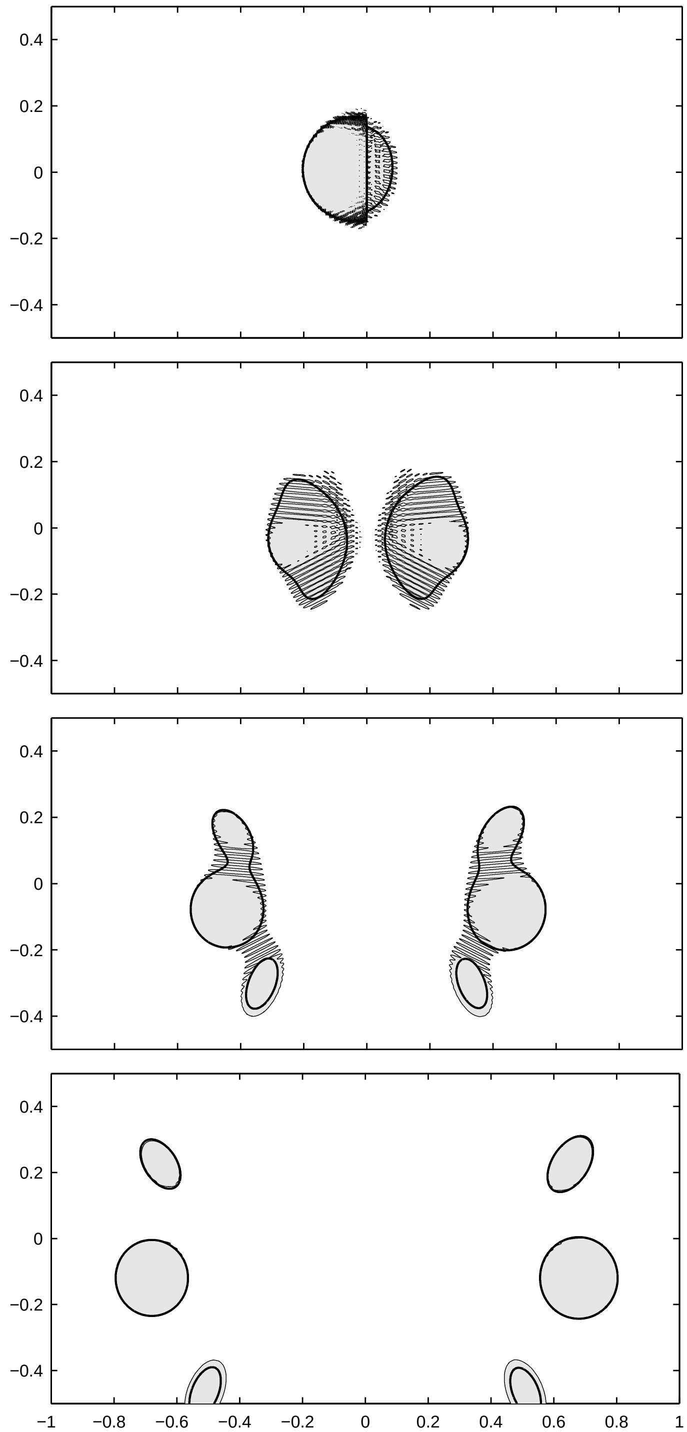

FIGURE 4.7. Contour plot of solution to Example 4.3.2 at $\rho(x, y) = 2$ for $\varepsilon = 800^{-1}$ at $t = 0.25$, 0.5, 0.75 and 1.0.The contour of the Schrödinger solution is filled in and the contour for numerical semiclassical limit is illustrated by a bold line.

Chapter 5

Extensions to the Model and Further Research

In this chapter we consider corrections to the semiclassical model as motivation and direction for future research. Since the goal of this chapter is to explore extrapolations to the ideas developed in previous chapters as a vehicle for future research, the results are presented without the same level of rigor as in previous chapters.

In developing the semiclassical model we imposed several limiting assumptions on the potential barrier. Namely, the width of the barrier is $O(\varepsilon)$, the distance between neighboring barriers is $O(1)$, the change in the potential $\nabla_x V(x)$ is $O(1)$ except at quantum barriers, and the coherence time is sufficiently short. Two notable potentials that are exceptions to these limitations are crystalline domains and mesoscopic barriers. Periodic crystalline domains, such as the Kronig-Penney model [26], consist of narrow, closely-spaced potential barriers or wells. Because the separation between neighboring barriers is $O(\varepsilon)$, the barriers may not be considered independent. Furthermore, since the barriers extend across the whole the domain, the classical region is effectively coupled into the quantum region. A mesoscopic barrier arises when the scaled Planck constant ε, while small, is nonvanishing or when the barrier width is substantially larger than the effective support of the quantum wavepacket. In this case, the barrier may not act like a single scatterer but rather like a series of multiple scatters.

As discussed in Section 2.3, the barrier scattering in the semiclassical model is a time-irreversible and entropy-increasing process because the interface condition is not one-to-one. That is, the interface condition combines information from multiple separate bicharacteristics. The Schrödinger equation, on the other hand, is time reversible. As discussed in Section 3.1.1, the transmission and reflection coefficients are computed by solving the Schrödinger equation in order to derive a quantum scattering matrix for the barrier

$$\mathsf{S}_{\mathcal{Q}} = \begin{pmatrix} r_1 & t_2 \\ t_1 & r_2 \end{pmatrix} \tag{5.1}$$

where r_j and t_j for $j = 1, 2$ are complex numbers. The complex-valued scattering matrix (3.5) contains not only information about scattering probabilities, but also the phase shift and ultimately the phase delay time. The semiclassical scattering matrix

$$\mathsf{S} = \begin{pmatrix} R_1 & T_2 \\ T_1 & R_2 \end{pmatrix} = \begin{pmatrix} |r_1|^2 & \frac{\kappa_1}{\kappa_2}|t_2|^2 \\ \frac{\kappa_2}{\kappa_1}|t_1|^2 & |r_2|^2 \end{pmatrix} \quad \text{where} \quad \kappa_i = \sqrt{p^2 - 2mV_i}$$

discards the phase information. Since we only track the particle density, the solution is decoherent away the barrier.

The difference between the semiclassical solution $f(x, p, t)$ and the Schrödinger solution $\psi(x, t)$ becomes evident by examining the position density $\rho(x, t)$. The Schrödinger equation and the Liouville equations are linear with respect to ψ and f, respectively. But the position density is only linear with respect to f. Consider ψ_1, ψ_2, f_1 and f_2 with $\rho_1 = \int f_1 \, dp = |\psi_1|^2$ and $\rho_2 = \int f_2 \, dp = |\psi_2|^2$. The position density for the superpositioned solutions $f_1 + f_2$ is $\rho_1 + \rho_2$, but the position density for the superpositioned solutions $\psi_1 + \psi_2$ is

$$\rho_1 + \rho_2 + 2\sqrt{\rho_1 \rho_2} \cos(\theta_1 - \theta_2) \tag{5.2}$$

where θ_j is the phase of ψ_j for $j = 1, 2$. The probability amplitude $\psi_1 + \psi_2$ contains an additional coherence term which is not captured by the semiclassical interface conditions (2.16) and (2.17). Hence, the physical observables of the semiclassical Liouville solution in general will not agree with the physical observables of the Schrödinger solution. This point was highlighted in Section 2.3 for the harmonic oscillator with a delta-function barrier. A natural correction to the semiclassical model is one that not only tracks density along the bicharacteristics but also phase-offset information from the barrier.

5.1 Coherent semiclassical model

In this section we shall consider a coherent semiclassical model and discuss the numerical implementation. In the limit as the scaled Planck constant $\varepsilon \to 0$, phase offset may not be well-defined if only because the semiclassical measurements cannot resolve quantum distances. Furthermore, since the solution is less likely to to exhibit coherence in two-dimensions, we limit the discussion to one dimension.

Define the semiclassical probability amplitude as

$$\Phi(x, p, t) = \sqrt{f(x, p, t)} e^{i\theta(p)}$$

where $\theta(p)$ is the phase offset from the initial conditions $\Phi(x,p,0) = \sqrt{f(x,p,0)}$. Define the coherent probability density as

$$f_{\text{coh}}(x,p,t) = |\Phi(x,p,t)|^2.$$

If $\Phi(x,p,t)$ satisfies the evolution equation

$$\frac{d\Phi}{dt} = \frac{\partial\Phi}{\partial t} + \frac{dx}{dt}\frac{\partial\Phi}{\partial x} + \frac{dp}{dt}\frac{\partial\Phi}{\partial p} = 0$$

then $f_{\text{coh}}(x,p,t)$ satisfies

$$\frac{\partial f_{\text{coh}}}{\partial t} + \frac{dx}{dt}\frac{\partial f_{\text{coh}}}{\partial x} + \frac{dp}{dt}\frac{\partial f_{\text{coh}}}{\partial p} = 0.$$

Hence, if $\Phi(x,p,t)$ is a solution to the Liouville equation for initial condition $\Phi(x,p,0)$ then $f_{\text{coh}}(x,p,t)$ is a solution to the Liouville equation for initial condition $f_{\text{coh}}(x,p,0)$. Furthermore, $|\Phi_1 + \Phi_2|^2 = f_1 + f_2 + 2\sqrt{f_1 f_2}\cos(\theta_1 - \theta_2)$. If f_{coh} is independent of p or if f_1 is a scalar multiple of f_2, then this condition is equivalent to condition (5.2).

When there are several bicharacteristics stemming from a scattering barrier, we define the semiclassical probability amplitude as the superposition

$$\Phi(x,p,t) = \sum_k s_k(H(x,p))\Phi_k(x,p,t)$$

where $\Phi_k(x,p,t)$ is the solution along the k-th bicharacteristic

$$\Phi_k(x,p,t) = \int \Phi(\tilde{x},\tilde{p},0)\varphi_k(x,p,t;\tilde{x},\tilde{p})\,d\tilde{x}\,d\tilde{p}$$

and kth global bicharacteristic for the Hamiltonian $H(\tilde{x},\tilde{p})$ is defined as

$$\varphi_k(x,p,t;\tilde{x},\tilde{p}) = \delta(x(t)-\tilde{x})\delta(p(t)-\tilde{p}).$$

We define scattering term $s_k(H(x,p))$ as the product of complex-valued transmission and reflection coefficients (5.1) along the kth bicharacteristic. The definition is similar to the superpositioning of the particle density of the semiclassical model Section 2.2, but in this case, it incorporates the linearity of the Schrödinger solution. Hence, we have the coherent probability density

$$f_{\text{coh}}(x,p,t) = \left|\sum_k s_k(H(x,p))\Phi_k(x,p,t)\right|^2.$$

We define the position density in the usual manner

$$\rho(x,t) = \int f_{\text{coh}}(x,p,t)\,dp.$$

Consider implementation of the coherent semiclassical model numerically using either the deterministic or the Monte Carlo particle method discussed in the preceding chapter. A first-order finite volume approach is analogous to the method discussed in Chapter 3 may also be constructed. In the deterministic particle approach, we take the weight

$$w_k = \int_{C_k} \Phi(x, p, 0)\, dx\, dp$$

for a cell C_k. At each node j record either $s_j = t$ or $s_j = r$ where t is the complex-valued transmission coefficient and r is the complex-valued reflection coefficient defined by the scattering matrix (3.5) for the barrier associated with the node. Take $\Phi_k(x^n, p^n, t^n) = \sum_j w_k \delta(x - x^n)\delta(p - p^n) \prod s_{k_j}$. Use the cutoff function (4.27) over phase space (x, p) to associate the Dirac measure $\delta(x - x^n)\delta(p - p^n)$ with the mesh (x_i, p_j). Finally, combine the results with the previous solution. In the Monte Carlo approach, we sample N particles randomly from $\Phi(x, p, 0)$ and take $w_n = N^{-1/2}$. At a barrier, define the transmission and reflection probabilities as usual $T = |t|^2$ and $R = |r|^2$. Sample a uniform random variable X. If $X < T$, the particle is transmitted; otherwise, the particle is reflected. Set $w_k \leftarrow t w_k / T$ for transmission and $w_k \leftarrow r w_k / R$. for reflection. Take $\Phi_k(x^n, p^n, t^n) = w_k \delta(x - x^n)\delta(p - p^n)$. Use the cutoff function (4.27) over phase space (x, p) to associate $\delta(x - x^n)\delta(p - p^n)$ with the mesh (x_i, p_j). Combine the results with the previous solution. The obvious shortcoming of the deterministic approach is that it is impractical to track all bicharacteristic branches for complicated geometries with several barriers, such as in a crystalline material. The shortcoming to the Monte Carlo approach is inherently *unstable* because of the rescaling.

As a simple example we compare the Schrödinger equation, the semiclassical model and the coherent semiclassical model for the harmonic oscillator with a delta-function barrier

$$V(x) = \tfrac{1}{2}x^2 + \varepsilon\alpha\delta(x)$$

introduced in Section 2.3. The complex-valued scattering coefficients for the delta-function barrier are [42]

$$t = \frac{ip}{ip - \alpha} \quad \text{and} \quad r = \frac{\alpha}{ip - \alpha}.$$

Let $\alpha = \sqrt{3}$ and take the Gaussian initial distribution

$$\psi(x,0) = (\pi\sigma^2)^{-1/4} \exp\left(-\frac{x-x_0}{2\sigma^2}\right) \exp\left(i\varepsilon^{-1}p_0 x\right)$$
$$f(x,p,0) = (\pi\varepsilon)^{-1} \exp\left(-\frac{(x-x_0)^2}{\sigma^2}\right) \exp\left(-\frac{(p-p_0)^2}{\varepsilon^2\sigma^{-2}}\right)$$
$$\Phi(x,p,0) = (\pi\varepsilon)^{-1/2} \exp\left(-\frac{(x-x_0)^2}{2\sigma^2}\right) \exp\left(-\frac{(p-p_0)^2}{2\varepsilon^2\sigma^{-2}}\right)$$

with $\varepsilon = 0.01$, $\sigma = 0.1$, $x_0 = 1$ and $p_0 = 0$. The semiclassical model is solved using the finite-volume method developed in Section 3.1.2 and the coherent semiclassical model is solved using the deterministic method. The Schrödinger equation is solved using the Crank-Nicolson scheme (3.16) with the delta-potential $\delta(x)$ approximated by $(\Delta x)^{-1}\delta_{i0}$. The coherent semiclassical model accurately describes the coherent behavior exhibited by the Schrödinger solution. The solutions are plotted in Figure 5.1 on the following page.

5.2 Conclusion and directions

Chapter 2 mentioned that conservation of energy, by providing a constraint on the solutions, creates an equivalence class of bicharacteristics but does not yield a unique solution. An interface condition based on the physical characteristics of the barrier was needed in order to isolate appropriate mixing. In Chapter 3 and Chapter 4 we implemented the model in the case of a decoherent interface condition. For the class of one and two-dimensional thin barriers, we demonstrated that the Schrödinger and the von Neumann solutions converge to the semiclassical Liouville solutions at a rate of $O(\varepsilon)$. Finally, we introduced a coherent semiclassical by modifying the interface condition.

While the coherent semiclassical model is valid for a limited set of problems, the existence of another model, consistent with the Hamiltonian preservation principle and with an interface condition that is as physically justifiable as the decoherent model, underscores the importance of choosing the appropriate interface condition. A wrong interface condition can only give a wrong solution. The future goal of this research is to overcome the shortcomings of the coherent semiclassical model and to develop a robust, viable model that serves as the logical first step to solving problems over periodic and mesoscopic potentials.

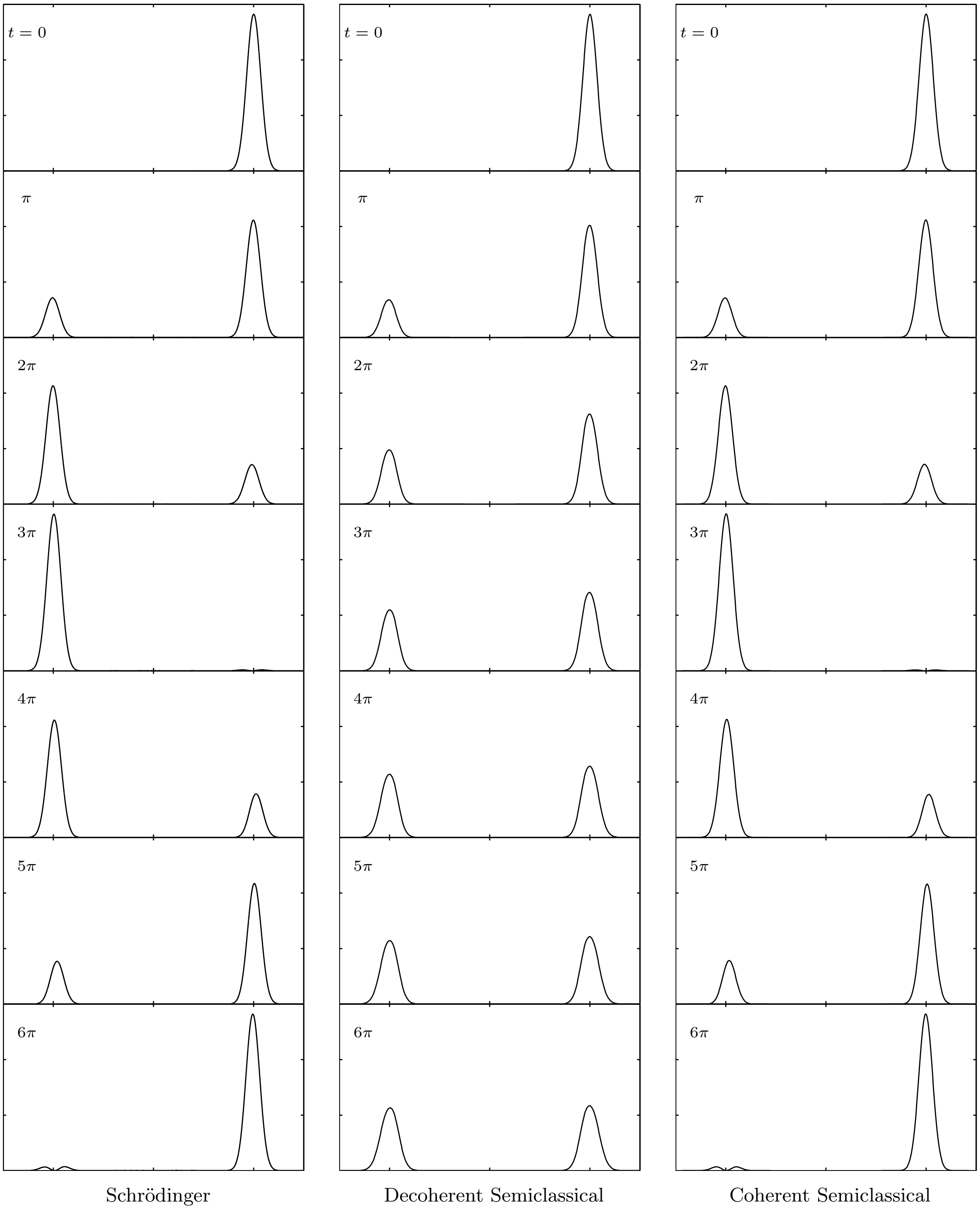

FIGURE 5.1. Comparison of Schrödinger, decoherent semiclassical, and coherent semiclassical solutions to the example in Section 5.1 at $t = 0$, π $\ldots$ 6π.

List of References

[1] Y. Ando and T. Itoh. Calculation of transmission tunneling current across arbitrary potential barriers. *J. Appl. Phys.*, 61(4):1497–1502, February 1987.

[2] A. Arnold. Mathematical concepts of open quantum boundary conditions. *Transport Theor. Stat.*, 30(4–6):561–584, 2001.

[3] G. Bal, J. B. Keller, G. Papanicolaou, and L. Ryzhik. Transport theory for acoustic waves with reflection and transmission at interfaces. *Wave Motion*, 30(4):303–327, 1999.

[4] W. Bao, S. Jin, and P. A. Markowich. On time-splitting spectral approximations for the Schrödinger equation in the semiclassical regime. *J. Comput. Phys.*, 175(2):487–524, 2002.

[5] W. Bao, S. Jin, and P. A. Markowich. Numerical study of time-splitting spectral discretizations of nonlinear Schrödinger equations in the semi-clasical regimes. *SIAM J. Sci. Comp.*, 25:27–64, 2003.

[6] N. Ben Abdallah. A hybrid kinetic-quantum model for stationary electron transport. *J. Stat. Phys.*, 90(3-4):627–662, 1998.

[7] N. Ben Abdallah, P. Degond, and I. M. Gamba. Coupling one-dimensional time-dependent classical and quantum transport models. *J. Math. Phys.*, 43(1):1–24, 2002.

[8] N. Ben Abdallah and S. Tang. On hybrid quantum-classical transport models. *Math. Methods Appl. Sci.*, 27(6):643–667, 2004.

[9] A. O. Bolivar. *Quantum-classical Correspondence*. The Frontiers Collection. Springer, New York, 2004.

[10] M. M. Dingham. Transfer-matrix approach to quantum transport in two-dimensional geometries. *Phys. Rev. B.*, 50(4):2241–2247, 1994.

[11] C. Eckart. The penetration of a potential barrier by electrons. *Phys. Rev.*, 35(11):1303–1309, June 1930.

[12] P. Gérard, P. A. Markowich, N. J. Mauser, and F. Poupaud. Homogenization limits and Wigner transforms. *Comm. Pure Appl. Math.*, 50(4):323–379, 1997.

[13] G. H. Golub and C. F. Van Loan. *Matrix Computations*. Johns Hopkins Studies in the Mathematical Sciences. Johns Hopkins University Press, Baltimore, MD, third edition, 1996.

[14] L. Gosse and N. J. Mauser. Multiphase semiclassical approximation of an electron in a one-dimensional crystalline lattice. III. From ab initio models to WKB for Schrödinger-Poisson. *J. Comput. Phys.*, 211(1):326–346, 2006.

[15] P. Grossel and J. M. Vigoureux. Nonlocal approach to scattering in a one-dimensional problem. *Phys. Rev. A*, 50(5):3627–3637, 1994.

[16] E. Hairer, C. Lubich, and G. Wanner. *Geometric Numerical Integration*, volume 31 of *Springer Series in Computational Mathematics*. Springer-Verlag, Berlin, 2002. Structure-preserving algorithms for ordinary differential equations.

[17] B. Hellsing and H. Metiu. An efficient method for solving the quantum Liouville equation: applications to electronic absorption spectroscopy. *Chem. Phys. Lett.*, 127(1):45–49, 1986.

[18] F. If, P. Berg, P. L. Christiansen, and O. Skovgaard. Split-step spectral method for nonlinear Schrödinger equation with absorbing boundaries. *J. Comput. Phys.*, 72:501–503, 1987.

[19] S. Jin and X. Li. Multi-phase computations of the semiclassical limit of the Schrödinger equation and related problems: Whitham vs. Wigner. *Phys. D*, 182(1-2):46–85, 2003.

[20] S. Jin and X. Wen. A Hamiltonian-preserving scheme for the Liouville equation of geometrical optics with transmissions and reflections. *SIAM J. Numer. Anal.* submitted.

[21] S. Jin and X. Wen. Hamiltonian-preserving schemes for the Liouville equation with discontinuous potentials. *Commun. Math. Sci.*, 3(3):285–315, 2005.

[22] S. Jin and X. Wen. Hamiltonian-preserving schemes for the Liouville equation of geometrical optics with discontinuous local wave speeds. *J. Comp. Phys.*, xxx(x):xxx–xxx, 2006.

[23] B. Jonsson and S. T. Eng. Solving the Schrödinger equation in arbitrary quantum-well potential profiles using the transfer-matrix method. *IEEE J. Quantum Elect.*, 726(11):2025–2035, November 1990.

[24] N. C. Kluksdahl, A. M. Kriman, D. K. Ferry, and C. A. Ringhofer. Self-consistent study of the resonant tunneling diode. *Phys. Rev. B.*, 39(11):7720–7735, 1989.

[25] R. Kosloff and D. Kosloff. Absorbing boundaries for wave propagation problems. *J. Comput. Phys.*, 63:363–376, 1986.

[26] R. de L. Kronig and W. G. Penney. Quantum mechanics of electrons in crystal lattices. *Proc. Roy. Soc. (London)*, A130:499–513, 1931.

[27] P. D. Lax. The flowering of applied mathematics in America. *SIAM Rev.*, 31(4):533–541, December 1989.

[28] C. S. Lent and D. J. Kirkner. The quantum transmitting boundary method. *J. Appl. Phys.*, 67(10):6353–6359, May 1990.

[29] R. J. Leveque. *Finite Volume Methods for Hyperbolic Problems*. Cambridge Texts in Applied Mathematics. Cambridge University Press, Cambridge, 2002.

[30] Shaofan Li and Wing Kam Liu. *Meshfree particle methods*. Springer-Verlag, Berlin, 2004.

[31] P.-L. Lions and T. Paul. Sur les mesures de Wigner. *Rev. Mat. Iberoamericana*, 9(3):553–618, 1993.

[32] V. A. Mandelstahm and H. S. Taylor. Spectral projection approach to the quantum scattering calculations. *J. Chem. Phys.*, 102(19):7390–7398, 1995.

[33] P. A. Markowich, P. Pietra, and C. Pohl. Numerical approximation of quadratic observables of Schrödinger-type equations in the semi-classical limit. *Numer. Math.*, 81(4):595–630, 1999.

[34] P. A. Markowich, C. A. Ringhofer, and C. Schmeiser. *Semiconductor Equations*. Springer-Verlag, Vienna, 1990.

[35] A. Messiah. *Quantum Mechanics. Vol. I.* Translated from the French by G. M. Temmer. North-Holland Publishing Co., Amsterdam, 1961.

[36] L. Miller. Refraction of high-frequency waves density by sharp interfaces and semiclassical measures at the boundary. *J. Math. Pures Appl. (9)*, 79(3):227–269, 2000.

[37] P.-A. Raviart. An analysis of particle methods. In *Numerical Methods in Fluid Dynamics (Como, 1983)*, volume 1127 of *Lecture Notes in Math.*, pages 243–324. Springer, Berlin, 1985.

[38] L. Ryzhik, G. C. Papanicolaou, and J. B. Keller. Transport equations for waves in a half space. *Comm. Partial Differential Equations*, 22(11-12):1869–1910, 1997.

[39] W.-D. Scheng. The scattering matrix method for quantum waveguides. *J. Phy.: Condens. Matter*, 9:8369–8380, 1997.

[40] C. Sparber, P. A. Markowich, and N. J. Mauser. Wigner functions versus WKB-methods in multivalued geometrical optics. *Asymptot. Anal.*, 33(2):153–187, 2003.

[41] J. P. Sun, G. I. Haddad, P. Mazumder, and J. N. Schulman. Resonant tunneling diodes: Modes and properties. *P. IEEE*, 86(4):641–661, 1998.

[42] J. S. Walker and J. Gathright. Exploring one-dimensional quantum-mechanics with transfer-matrices. *American Journal of Physics*, 62(5):408–422, 1994.

[43] E. Wigner. On the quantum correction for thermodynamic equilibrium. *Phys. Rev.*, 40(5):749–759, June 1932.